ELSEVIER

Contents lists available at ScienceDirect

Advances in Engineering Software

journal homepage: www.elsevier.com/locate/advengsoft





Optimal local truncation error method for solution of 3-D Poisson equation with irregular interfaces and unfitted Cartesian meshes as well as for post-processing

A. Idesman*, M. Mobin

Department of Mechanical Engineering, Texas Tech University, Lubbock, TX 79409-1021, USA

ARTICLE INFO

Keywords: Poisson equation with discontinuous coefficients Irregular interfaces Unfitted Cartesian meshes Optimal accuracy Post-processing Spatial derivatives

ABSTRACT

Recently the optimal local truncation error method (OLTEM) has been developed for the 2-D Poisson equation for heterogeneous materials with irregular interfaces and unfitted Cartesian meshes. Here we extend it to the general 3-D case. 27-point stencils that are similar to those for linear finite elements are used with OLTEM. The interface conditions at a small number of selected interface points where the jumps in material properties occur are added to the expression for the local truncation error and do not change the width of the stencils. There are no unknowns on interfaces between different materials; the structure of the global discrete equations is the same for homogeneous and heterogeneous materials. The calculation of the unknown stencil coefficients is based on the minimization of the local truncation error of the stencil equations, includes the entire PDE for the derivations and yields the optimal third order of accuracy of OLTEM with the 27-point stencils. The 3-D numerical results for heterogeneous materials with irregular interfaces and different material contrasts show that at the same number of degrees of freedom, OLTEM is even much more accurate than high-order (up to the 6th order) finite elements with much wider stencils. Compared to linear finite elements with similar 27-point stencils, at the engineering accuracy of 0.1% OLTEM decreases the number of degrees of freedom by a factor of greater than 3500. This leads to a huge reduction in computation time.

For the first time, a new post-processing procedure has been developed with OLTEM for the calculation of the spatial derivatives of numerical solutions. The spatial derivatives for each grid point are calculated with the help of one compact 27-point stencil (the same as for basic computations) for the corresponding grid point and the use of the original PDE. The spatial derivatives of the OLTEM solutions calculated with the new post-processing procedure are much more accurate compared to those obtained by high-order (up to the 7th order) finite elements with much wider stencils. At the engineering accuracy of 0.1% for the spatial derivatives, OLTEM decreases the number of degrees of freedom by a factor of greater than 10⁶ compared to linear finite elements. The new post-processing procedure can be equally applied to the calculation of the partial derivatives obtained by other numerical methods as well as to the numerical results for other PDEs.

Due to the huge reduction in the computation time compared to existing methods and the use of trivial unfitted Cartesian meshes that are independent of irregular geometry, the proposed technique does not require remeshing for the shape change of irregular geometry and it will be effective for many design and optimization problems as well as for multiscale problems without the scale separation.

1. Introduction

The Poisson equation for heterogeneous materials with interfaces is used for the description of many important phenomena such as heat transfer, multiphase flows, neurosciences, electrostatics and many others. Therefore, many efforts are made for the development of

accurate and computationally efficient numerical techniques for this equation; e.g., see [1-10] and many others. The finite element method, the finite volume method, the isogeometric elements, the spectral elements and similar techniques represent very powerful tools for the solution of partial differential equations (PDEs) for a complex geometry. However, the generation of non-uniform meshes for a complex geometry

E-mail address: alexander.idesman@ttu.edu (A. Idesman).

^{*} Corresponding author.

is not simple and may lead to the decrease in accuracy of these techniques if 'bad' elements (e.g., elements with small angles) appear in the mesh. Moreover, the conventional derivation of discrete equations for these techniques (e.g., based on the Galerkin approaches) does not lead to the optimal accuracy. There is a significant number of publications related to numerical techniques for different PDEs on irregular domains with uniform embedded meshes. For example, we can mention the following fictitious domain numerical methods that use uniform embedded meshes: the embedded finite difference method, the cut finite element method, the finite cell method, the Cartesian grid method, the immersed interface method, the virtual boundary method, the embedded boundary method, etc. The main objective of these techniques is to simplify the mesh generation for irregular domains as well as to mitigate the effect of 'bad' elements. For example, the techniques based on the finite element formulations (such as the cut finite element method, the finite cell method, the virtual boundary method and others) yield the p+1 order of accuracy even with small cut cells generated due to complex irregular boundaries (e.g., see [11-17] and many others). The main advantage of the embedded boundary method developed in [18–22] is the use of simple Cartesian meshes. The boundary conditions or fluxes in this technique are interpolated using the Cartesian grid points and this leads to the increase in the stencil width for the grid points located close to the boundary (the numerical techniques developed in [18-22] provide just the second order of accuracy for the global solution). A stable generalized finite element method for the Poisson equation was developed in [7] for heterogeneous materials with curved interfaces and unfitted uniform meshes. The second order of accuracy in the energy norm was achieved in [7] with 2-D quadratic finite elements that form 25-point stencils. The order of accuracy p + 1 for interface problems for the Poisson equation on unfitted meshes was reported in [10,23-26] for high-order immersed and extended finite elements of order p.

The development of robust numerical techniques for the solution of PDEs with complex irregular interfaces that provide an optimal and high order of accuracy is still a challenging problem.

Recently we have developed OLTEM with compact stencils for the solution of PDEs with constant coefficients (homogeneous materials) on regular and irregular domains (e.g., see [27–33]) as well as OLTEM with compact stencils for the solution of the scalar wave, heat and Poisson equations in the 2-D case for heterogeneous materials with irregular interfaces (see [34,35]). The main advantages of OLTEM are the optimal accuracy of discrete equations and the use of unfitted Cartesian meshes for irregular geometry. For many existing techniques the optimal accuracy of the discrete equations even is not known. For example, we already mentioned that finite elements of order p provide the p+1 order of accuracy. However, in our papers [30,33] we showed that for the same structure of the discrete equations, quadratic elements (p=2) provide the 18th order of accuracy for the Poisson equation and the 10th order of accuracy for the elasticity equations on regular domains with uniform meshes.

In this paper, we extend OLTEM developed in our paper [35] for the 2-D Poisson equation with heterogeneous materials to the general 3-D case. It is known that the transition from the 2-D geometry to the 3-D geometry is a challenging problem due to the complexity of 3-D irregular geometry. Due to the complexity of analytical expressions of OLTEM, their derivations for the 3-D Poisson equation with irregular interfaces is also a challenge (see also Remark 4 below). Another novelty of the paper is the development of a new post-processing procedure for the accurate calculations of the spatial derivatives of numerical solutions. For example, it is known that due to piecewise continuous shape functions of conventional finite elements, the spatial derivatives are discontinuous across finite element boundaries and special post-processing procedures are necessary for their accurate calculations; e.g., see [36–38]. Here we show that OLTEM with compact stencils can accurately calculate the spatial derivatives of numerical solutions as well. The proposed post-processing procedure developed here for the

Poisson equation can be also extended to different PDEs (e.g., for the calculation of stresses for the elasticity equations) as well as it can be applied to other techniques (e.g., for post-processing finite element results).

The Poisson equation in a composite domain $\Omega = \cup \Omega_l$ $(l=1,2,...,\overline{N})$ where \overline{N} is the total number of subdomains) can be written down in each subdomain Ω_l as follows:

$$e_l \nabla^2 u_l = f_l \,, \tag{1}$$

where e_l is a constant in each subdomain Ω_l and can be discontinuous across the interfaces between subdomains Ω_l ($l=1,2,...,\overline{N}$), $f_l(x)$ is the source term that can be also discontinuous across the interfaces between subdomains Ω_l , u_l is the field variable. We also assume that the functions u_l and f_l are sufficiently smooth in each subdomain Ω_l . At the interface G between any two subdomains, the following interface conditions (the continuity of the function and the flux across the interface) are applied:

$$u_{G}^{*} - u_{G}^{**} = 0, \ e_{*} \left(n_{x} \frac{\partial u_{G}^{*}}{\partial x} + n_{y} \frac{\partial u_{G}^{*}}{\partial y} + n_{z} \frac{\partial u_{G}^{*}}{\partial z} \right) - e_{**} \left(n_{x} \frac{\partial u_{G}^{**}}{\partial x} + n_{y} \frac{\partial u_{G}^{**}}{\partial y} + n_{z} \frac{\partial u_{G}^{**}}{\partial z} \right) = 0,$$
(2)

where n_x , n_y and n_z are the x-, y- and z-components of the normal vector at the interface, e_* (e_{**}) is the corresponding material constant, the symbols * and ** correspond to the quantities on the opposite sides from the interface for the corresponding subdomains Ω_l . This means that the functions u_l are continuous across the interfaces but can have the discontinuous spatial derivatives across the interfaces.

Remark 1. The derivations for the new approach can be easily extended to the case with the discontinuous functions and fluxes across interfaces; i.e., when the right-hand sides in Eq. (2) are the given functions. However, for simplicity we consider Eq. (2) with zero right-hand sides.

In this paper the Dirichlet boundary conditions $u=g_1$ are applied along the boundary Γ where g_1 is the given function. However, the Neumann boundary conditions can be also used with the proposed approach; e.g., see our paper [39]. According to OLTEM, the discrete system for the Poisson equation after the space discretization with a Cartesian rectangular mesh can be represented as a system of algebraic equations. The algebraic equation of this system for each internal grid point of the domain is called the stencil equation and can be written down for the case without interfaces as follows:

$$\sum_{i=1}^{M} k_i u_i^{num} = \bar{f} \,, \tag{3}$$

where u_i^{num} is the numerical solution for function u_i at the grid points, k_i are the unknown stencil coefficients to be determined, \overline{f} is the discretized source term (see the next Sections), M is the number of the grid points included into the stencil equation. Many numerical techniques such as the finite difference method, the finite element method, the finite volume method, the isogeometric elements, the spectral elements, different meshless methods and others can be finally reduced to Eq. (3) with some specific coefficients k_i . In the derivations below, we will assume 27-point (M=27) stencils in the 3-D case that are similar to 27-point stencils of 3-D linear quadrilateral finite elements on Cartesian meshes. Generally, the stencils with any number of points M can be used with the suggested approach.

Let us introduce the local truncation error used with OLTEM. The replacement of the numerical values of function u_i^{num} at the grid points in Eq. (3) by the exact solution u_i to the Poisson equation, Eq. (1), leads to the residual e of this equation called the local truncation error of the discrete equation, Eq. (3):

$$e = \sum_{i=1}^{M} k_i u_i - \overline{f} . \tag{4}$$

Calculating the difference between Eqs. (4) and (3) we can get

$$e = \sum_{i=1}^{M} k_{i} [u_{i} - u_{i}^{num}] = \sum_{i=1}^{M} k_{i} \overline{e}_{i}^{u},$$
 (5)

where $\overline{e}_i^u = u_i - u_i^{num}$ are the errors of function u_i at the grid points i. As can be seen from Eq. (5), the local truncation error e is a linear combination of the errors of the function u at the grid points i which are included into the stencil equation.

In Section 2.1, OLTEM with 27-point stencils is derived for the 3-D Poisson equation with discontinuous coefficients and zero source term. Its extension to nonzero source term is considered in Section 2.2. The development of OLTEM for the calculation of the spatial derivatives of numerical solutions (post-processing) is presented in Section 3. Numerical examples for a 3-D domain with an irregular interface and unfitted Cartesian meshes as well as the comparison with FEM are presented in Section 4. For the derivation of many analytical expressions presented below we use the computational program "Mathematica".

2. OLTEM for the 3-D Poisson equation with discontinuous coefficients

2.1. Zero source term $f_l = 0$ in Eq. (1)

Let us consider a 3-D bounded domain and a Cartesian rectangular mesh with a mesh size h where h is the size of the mesh along the x – axis, $b_y h$, $b_z h$ ares the sizes of the mesh along the y – and z – axes (b_y and b_z are the aspect ratios of the mesh). To simplify derivations, below we consider regular rectangular domains with irregular interfaces between different materials. However, irregular domains can be also considered with OLTEM; see [27-29]. In the paper we will consider 27-point uniform stencils that are similar to those for linear quadrilateral finite elements. We should mention that we use the same structure of stencils for homogeneous and composite materials (the difference between homogeneous and composite materials is in the values of the stencil coefficients only). The spatial locations of the 26 degrees of freedom that are close to the internal degree of freedom u_{14} and contribute to the 27-point stencil for this degree of freedom are shown in Fig. 1. For convenience, the local numeration of the grid points from 1 to 27 is used in Fig. 1 as well as in the derivations below. If all grid points of the 27-point stencil belong to the same material than this stencil is treated as that for homogeneous materials (see Fig. 1a) otherwise as for

heterogeneous materials (see Fig. 1b). The interface in Fig. 1b divides the 27-point uniform stencil into two parts with different material properties. In order to impose the interface conditions at the interface, we select a small number of interface points as follows. First we select one point at the interface with the coordinates $x_G = x_{G,1}$, $y_G = y_{G,1}$ and $z_G = z_{G,1}$. This point can be selected as the shortest distance from the internal grid point u_{14} of the 27-point stencil to the interface. Then, we additionally select 24 interface points in two perpendicular directions; i. e., we use totally $N_G = 25$ interface points for each stencil with interfaces. We distances $\overline{h} =$ same $\sqrt{(x_{G,j} - x_{G,i})^2 + (y_{G,j} - y_{G,i})^2 + (z_{G,j} - z_{G,i})^2}$ between the interface points where *i* and *j* designate the neighboring interface points; e.g., see Fig. 1b (we are not able to show all 25 interface points in Fig. 1b). The numerical experiments show that small distances $\overline{h} = h/5$ yield accurate

Let us describe the coordinates of the grid points of the 27 point uniform stencils (see Fig. 1) with respect to their central point u_{14} for the 27-point stencils as follow:

$$x_p = x_{14} + r_{x,p}h = x_{14} + (i-2)h,$$
 $y_p = y_{14} + r_{y,p}b_yh$
= $y_{14} + (j-2)b_yh,$ $z_p = z_{14} + r_{z,p}b_zh = z_{14} + (t-2)b_zh,$ (6)

for the 27-point stencils where the coefficients $r_{x,p}, r_{y,p}, r_{z,p}$ are:

$$r_{x,p} = (i-2), r_{y,p} = (j-2), r_{z,p} = (t-2),$$
 (7)

and
$$p = 9(t-1) + 3(j-1) + i$$
 with $i, j, t = 1, 2, 3$.

To describe the coordinates of the selected N_G points on the interface (see Fig. 1b) we introduce $3N_G$ coefficients $d_{x,p}$, $d_{y,p}$ and $d_{z,p}$ ($p=1,2,...,N_G$) with $N_G=25$ for the 27-point stencils as follows (see also Fig. 1b):

$$x_{Gj} = x_G + d_{xj}h$$
, $y_{Gj} = y_G + d_{yj}b_yh$, $z_{Gj} = z_G + d_{zj}b_zh$, j
= 1,2,..., N_G . (8)

where $d_{x,1} = d_{y,1} = d_{z,1} = 0$ for the central interface point $G = G_1$ with the coordinates $x_G = x_{G,1}$, $y_G = y_{G,1}$ and $z_G = z_{G,1}$; see Fig. 1b.

Remark 2. Some of the interface points G_i ($i = 1, 2, ..., N_G$) can be located slightly outside the 27-point cells. The derivations presented below are also valid for these cases.

The stencil equation, Eq. (3), for composite materials with the 27-

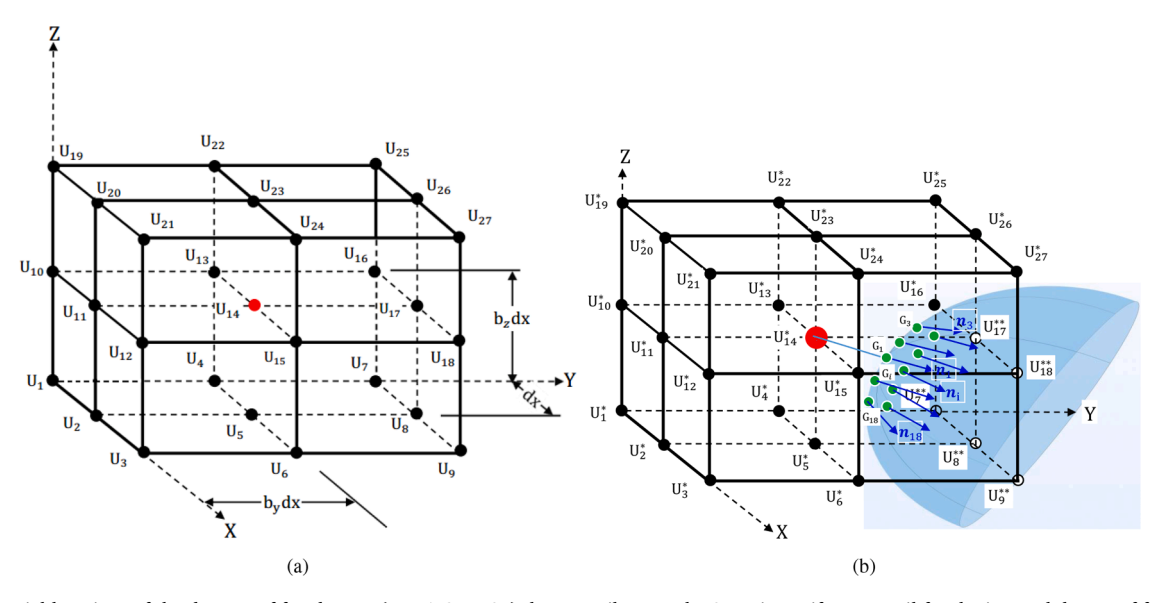


Fig. 1. The spatial locations of the degrees of freedom u_p (p = 1, 2, ..., 27) that contribute to the 27-point uniform stencil for the internal degree of freedom u_{14} for homogeneous material without interface (a) and for heterogeneous material with interface (b).

point uniform stencil for the grid point u_{14} (see Fig. 1) will be assumed in the following form:

$$\sum_{p=1}^{27} k_p \left[a_p u_p^{*,num} + (1 - a_p) u_p^{**,num} \right] = \overline{f},$$
 (9)

where $\bar{f}=0$ in the case of zero source $f_l=0$ in Eqs (1), the unknown stencil coefficients k_p (p=1,2,...,27) are to be determined from the minimization of the local truncation error, the coefficients $a_p=1$ if the grid point u_p belongs to material * or $a_p=0$ if the grid point u_p belongs to another material ** (i.e., only one variable $u_p^{*,num}$ or $u_p^{**,num}$ is actually included into Eq. (9) for each grid point; e.g., the coefficients a_p for Fig. 1b are: $a_l=1$ (l=1,2,...,6,10,11,...,16,19,20,...,27) and $a_l=0$ (l=7,8,9,17,18)). The local truncation error e follows from Eq. (9) by the replacement of the numerical solution $u_p^{*,num}$ and $u_p^{**,num}$ by the exact solution u_p^{*} and u_p^{**} :

$$e = \sum_{p=1}^{27} k_p \left[a_p u_p^* + (1 - a_p) u_p^{**} \right] - \overline{f} . \tag{10}$$

proposed method for general geometry of interfaces; see below.

Remark 3. Only $27 + 2N_G - 1$ out of the $27 + 2N_G$ coefficients k_p , $q_{1,j}$, $q_{2,j}$ (p = 1, 2, ..., 27, $j = 1, 2, ..., N_G$) in Eq. (11) can be considered as unknown coefficients. This can be explained as follows. In the case of zero source $f_l = 0$ and $\bar{f} = 0$, Eq. (9) can be rescaled by the division of the left- and right-hand sides of Eq. (9) by any scalar; i.e., one of the coefficients k_p can be selected as unity and there will be only $27 + 2N_G - 1$ unknown rescaled coefficients. The case of nonzero load $\bar{f} \neq 0$ can be similarly treated because the term \bar{f} is a linear function of the stencil coefficients; see below. For convenience, we will scale the stencil coefficients in such a way that k_{14} is $k_{14} = 1$.

In order to represent the local truncation error e as a Taylor series, let us expand the exact solution at the grid points and at the N_G selected interface points in Eq. (11) into a Taylor series at small $h \ll 1$ in the vicinity of the central interface point G for the 27-point stencils as follows:

$$v_{p} = v_{G} + \frac{\partial v_{G}}{\partial x} \left[(r_{x,p} - dx_{G})h \right] + \frac{\partial v_{G}}{\partial y} \left[(r_{y,p} - dy_{G})b_{y}h + \frac{\partial v_{G}}{\partial z} \left[(r_{z,p} - dz_{G})b_{z}h \right] + \frac{\partial^{2}v_{G}}{\partial x^{2}} \frac{\left[(r_{x,p} - dx_{G})h \right]^{2}}{2!} + \frac{\partial^{2}v_{G}}{\partial y^{2}} \frac{\left[(r_{y,p} - dy_{G})b_{y}h \right]^{2}}{2!} + \frac{\partial^{2}v_{G}}{\partial z^{2}} \frac{\left[(r_{z,p} - dz_{G})b_{z}h \right]^{2}}{2!} + 2\frac{\partial^{2}v_{G}}{\partial x^{2}} \frac{\left[(r_{x,p} - dx_{G})h \right] \left[(r_{y,p} - dy_{G})b_{y}h \right]}{2!} + ..., p = 9(t-1) + 3(j-1) + i \text{ with } i, j, t = 1, 2, 3$$

$$(12)$$

One of the ideas of the new approach is to include the interface conditions for the exact solution at a small number N_G of the interface points

with $dx_G = \frac{x_G - x_{14}}{h}$, $dy_G = \frac{y_G - y_{14}}{h \cdot h}$, and $dz_G = \frac{z_G - z_{14}}{h \cdot h}$, and

$$w_{j} = w_{G} + \frac{\partial w_{G}}{\partial x} \left[d_{xj} h \right] + \frac{\partial w_{G}}{\partial y} \left[d_{yj} b_{y} h \right] + \frac{\partial w_{G}}{\partial z} \left[d_{zj} b_{z} h \right] + \frac{\partial^{2} w_{G}}{\partial x^{2}} \frac{\left[d_{xj} h \right]^{2}}{2!} + \frac{\partial^{2} w_{G}}{\partial z^{2}} \frac{\left[d_{zj} b_{z} h \right]^{2}}{2!} + 2 \frac{\partial^{2} w_{G}}{\partial x^{2} y} \frac{\left[(d_{xj} h) \left[(d_{xj} h) \left((d_{xj} h) \left[(d_{xj} h) \left[(d_{xj} h) \left((d_{xj} h)$$

in the expression for the local truncation error in Eq. (10) as follows:

$$e = \sum_{p=1}^{27} k_p \left[a_p u_p^* + (1 - a_p) u_p^{**} \right]$$

$$+ \left\{ \sum_{j=1}^{N_G} q_{1,j} \left(u_{G,j}^* - u_{G,j}^{**} \right) + \sum_{j=1}^{N_G} h q_{2,j} \left[e_* \left(n_{x,j} \frac{\partial u_{G,j}^*}{\partial x} + n_{y,j} \frac{\partial u_{G,j}^*}{\partial y} + n_{z,j} \frac{\partial u_{G,j}^*}{\partial z} \right) \right.$$

$$- e_{**} \left(n_{x,j} \frac{\partial u_{G,j}^{**}}{\partial x} + n_{y,j} \frac{\partial u_{G,j}^{**}}{\partial y} + n_{z,j} \frac{\partial u_{G,j}^{**}}{\partial z} \right) \right] \right\} - \overline{f} ,$$

$$(11)$$

where $n_{x,j}$, $n_{y,j}$ and $n_{z,j}$ are the x-, y-, and z-components of the normal vectors at the N_G selected interface points (e.g., see Fig. 1b), the coefficients $q_{1,j}$ and $q_{2,j}$ ($j=1,2,...,N_G$) are unknown and will be used for the minimization of the local truncation error in Eq. (11) (see Section 2.1.2 below), the expressions in parenthesis after $q_{1,j}$ and $q_{2,j}$ are the interface conditions at the N_G selected interface points. Therefore, the expression in the curled brackets in Eq. (11) is zero (see Eq. (2)) and Eqs. (10) and (11) yield the same local truncation error e. The addition of the interface conditions at N_G points in Eq. (11) with the unknown coefficients $q_{1,j}$, $q_{2,j}$ ($j=1,2,...,N_G$) allows us to get a high accuracy of the

In Eq. (12) the function v_p is u_p^* , u_p^{**} , in Eq. (13) the function w_j is $u_{G,j}^*$, $u_{G,j}^{**}$, $\frac{\partial u_{G,j}^*}{\partial x}$, $\frac{\partial u_{G,j}^*}{\partial y}$, $\frac{\partial u_{G,j}^*}{\partial y}$, $\frac{\partial u_{G,j}^*}{\partial y}$, $\frac{\partial u_{G,j}^*}{\partial z}$, $\frac{\partial u_{G,j}^*}{\partial z}$, $\frac{\partial u_{G,j}^*}{\partial z}$, and $N_G=25$. The exact solution u_m^* and u_m^* to the Poisson equations, Eq. (1), at the central interface point $x=x_G$, $y=y_G$ and $z=z_G$ meets the following equations:

$$\frac{\partial^{2} u_{G}^{*}}{\partial x^{2}} = -\frac{\partial^{2} u_{G}^{*}}{\partial v^{2}} - \frac{\partial^{2} u_{G}^{*}}{\partial z^{2}} + \frac{1}{e_{s}} f^{*}, \qquad \frac{\partial^{2} u_{G}^{**}}{\partial x^{2}} = -\frac{\partial^{2} u_{G}^{**}}{\partial v^{2}} - \frac{\partial^{2} u_{G}^{**}}{\partial z^{2}} + \frac{1}{e_{s}} f^{**}, \qquad (14)$$

$$\begin{split} \frac{\partial^{(i+j+t+2)} u_{G}^{*}}{\partial z^{i} \partial y^{i} \partial x^{(2+j)}} &= -\frac{\partial^{(i+j+t+2)} u_{G}^{*}}{\partial z^{i} \partial y^{(i+2)} \partial x^{j}} - \frac{\partial^{(i+j+t+2)} u_{G}^{*}}{\partial z^{(t+2)} \partial y^{i} \partial x^{j}} + \frac{1}{e_{*}} \frac{\partial^{(i+j+t)} f^{*}}{\partial z^{i} \partial y^{j} \partial x^{j}}, \\ \frac{\partial^{(i+j+t+2)} u_{G}^{*}}{\partial z^{i} \partial y^{j} \partial x^{(2+j)}} &= -\frac{\partial^{(i+j+t+2)} u_{G}^{*}}{\partial z^{i} \partial y^{(i+2)} \partial x^{j}} - \frac{\partial^{(i+j+t+2)} u_{G}^{*}}{\partial z^{(t+2)} \partial y^{j} \partial x^{j}} + \frac{1}{e_{**}} \frac{\partial^{(i+j+t)} f^{**}}{\partial z^{i} \partial y^{j} \partial x^{j}} \end{split}$$
(15)

with $i,j,t=0,1,2,3,4,\ldots$ Eq. (15) is obtained by the differentiation of Eq. (14) with respect to x,y and z. Inserting Eqs. (12)–(15) with zero source term $f^*=f^{**}=0$ into Eq. (11) we get the following local truncation error in space e:

$$e = b_{1}u_{G}^{*} + b_{2}u_{G}^{**} + b_{4}u_{G}^{**} + b_{4}\frac{\partial u_{G}^{**}}{\partial z} + b_{5}\frac{\partial u_{G}^{**}}{\partial y} + b_{6}\frac{\partial u_{G}^{**}}{\partial y} + b_{7}\frac{\partial u_{G}^{**}}{\partial x} + b_{8}\frac{\partial u_{G}^{**}}{\partial x} + b_{1}\frac{\partial^{2}u_{G}^{**}}{\partial z^{2}} + b_{1}\frac{\partial^{2}u_{G}^{**}}{\partial z^{2}} + b_{10}\frac{\partial^{2}u_{G}^{**}}{\partial z^{2}} + b_{11}\frac{\partial^{3}u_{G}^{**}}{\partial z\partial y^{2}} + b_{12}\frac{\partial^{3}u_{G}^{**}}{\partial z\partial y^{2}} + b_{13}\frac{\partial^{2}u_{G}^{*}}{\partial y^{2}} + b_{14}\frac{\partial^{2}u_{G}^{**}}{\partial y^{2}} + b_{15}\frac{\partial^{3}u_{G}^{**}}{\partial z\partial x^{2}} + b_{16}\frac{\partial^{3}u_{G}^{**}}{\partial z\partial x^{2}} + b_{17}\frac{\partial^{2}u_{G}^{**}}{\partial x\partial y} + b_{18}\frac{\partial^{2}u_{G}^{**}}{\partial x\partial y} + b_{19}\frac{\partial^{3}u_{G}^{**}}{\partial z^{3}} + b_{20}\frac{\partial^{3}u_{G}^{**}}{\partial z^{3}} + b_{20}\frac{\partial^{3}u_{G}^{**}}{\partial z^{3}} + b_{20}\frac{\partial^{3}u_{G}^{**}}{\partial z^{3}} + b_{21}\frac{\partial^{3}u_{G}^{**}}{\partial z^{2}\partial y} + b_{22}\frac{\partial^{3}u_{G}^{**}}{\partial z\partial y\partial y} + b_{24}\frac{\partial^{3}u_{G}^{**}}{\partial z\partial y^{2}} + b_{25}\frac{\partial^{3}u_{G}^{**}}{\partial y^{3}} + b_{26}\frac{\partial^{3}u_{G}^{**}}{\partial y^{3}} + b_{26}\frac{\partial^{3}u_{G}^{**}}{\partial y^{3}} + b_{27}\frac{\partial^{3}u_{G}^{**}}{\partial z^{2}\partial x} + b_{29}\frac{\partial^{3}u_{G}^{**}}{\partial z\partial y\partial x} + b_{30}\frac{\partial^{3}u_{G}^{**}}{\partial z\partial y\partial x} + b_{31}\frac{\partial^{3}u_{G}^{**}}{\partial x\partial y^{2}} + b_{32}\frac{\partial^{3}u_{G}^{**}}{\partial x\partial y^{3}} + b_{30}\frac{\partial^{3}u_{G}^{**}}{\partial z\partial y\partial x} + b_{30}\frac{\partial^{4}u_{G}^{**}}{\partial x\partial y^{3}} + b_{50}\frac{\partial^{4}u_{G}^{**}}{\partial x\partial y^{3}} + b_{50}\frac{\partial^{6}u_{G}^{**}}{\partial x\partial y^{5}} + b_{98}\frac{\partial^{6}u_{G}^{**}}{\partial x\partial y^{5}} + b_{70}\left(h^{7}\right)$$

where the coefficients b_p (p=1,2,...) are expressed in terms of the coefficients k_i and $q_{1,j}$, $q_{2,j}$ ($i=1,2,...,27, j=1,2,...,N_G$) and are given in Appendix A. Here we should mention that the expression for the local truncation error, Eq. (16), includes only the first order derivatives with respect to x (the higher order derivatives with respect to x are excluded with the help of Eqs. (14)-(15)).

2.1.1. Homogeneous materials (without interface)

For homogeneous materials all a_j (j=1,2,...,27) coefficients are $a_j=1$ (see Eq. (9) if we consider material *) as well as all $q_{1,j}=q_{2,j}=0$ $(j=1,2,...,N_G)$ are zero. In this case the derivation of the local truncation error is similar to that in the previous section with $b_p=0$ (p=2,4,6,8,...) in Eq. (16) if we consider material *. The stencils coefficients k_i (i=1,2,...,27) can be analytically found from the following system of 27 algebraic equations:

$$b_p = 0, p = 1, 3, 5, 7, 9, 11, 13, 15, 17, 19, 21, 23, 25, 27, 29, 31, 33, 35, 37, 41, 45, 47, 53, 55, 67, 77$$
 (17)

$$k_{14} = 1 (18)$$

and they are:

$$k_{1} = -\frac{(5(b_{z}^{2}+1)b_{y}^{2}+5b_{z}^{2}+9)}{8(125(b_{z}^{2}+1)b_{y}^{2}+125b_{z}^{2}+9)}, \qquad k_{2}$$

$$= \frac{(5(b_{z}^{2}-5)b_{y}^{2}-25b_{z}^{2}+9)}{500(b_{z}^{2}+1)b_{y}^{2}+500b_{z}^{2}+36}, \dots$$
(19)

(see Appendix C for the expressions for the all stencil coefficients k_i , i = 1, 2, ..., 27) with the following local truncation error (see our paper [29] for details):

$$e = \frac{3b_y^2 b_z^2 h^6}{8\left(9 + 125\left(b_z^2 + b_y^2 + b_y^2 b_z^2\right)\right)}$$

$$\left[\left(-1 + b_y^4\right) \frac{\partial^6 u_{14}}{\partial y^6} + \left(-1 + b_z^4\right) \frac{\partial^6 u_{14}}{\partial z^6}\right]$$

$$+ \frac{b_y^2 b_z^2 h^8}{672\left(9 + 125\left(b_z^2 + b_y^2 + b_y^2 b_z^2\right)\right)} \left[\left(11 - 21b_y^2 - 21b_y^4 + 11b_y^6\right) \frac{\partial^8 u_{14}}{\partial y^8}$$

$$+ \left(-19 - 21b_z^2 + 21b_y^4\left(-1 + b_z^2\right)\right) \frac{\partial^8 u_{14}}{\partial y^6 \partial z^2} - 60 \frac{\partial^8 u_{14}}{\partial y^4 \partial z^4} + \left(-19 - 21b_z^4 + 21b_y^2\left(-1 + b_z^4\right)\right) \frac{\partial^8 u_{14}}{\partial y^2 \partial z^6} + \left(11 - 21b_z^2 - 21b_z^4 + 11b_z^6\right) \frac{\partial^8 u_{14}}{\partial z^8}\right] + O(h^{10}).$$

$$(20)$$

As can be seen from Eq. (20), for homogeneous materials and cubic ($b_y=b_z=1$) Cartesian meshes the local truncation error is two order higher compared to that for rectangular ($b_y\neq 1$ or/and $b_z\neq 1$) Cartesian meshes.

2.1.2. Heterogeneous materials with an irregular interface

For the interface represented by an inclined plane, some analytical results for the 27-point stencils that include the grid points with different material properties can be obtained with the help of Mathematica. We have found that the maximum order of the local truncation error for the 27-point stencils is 4. In order to obtain the same order of accuracy for the general shape of the interface we will use the following procedure.

We use the 76 unknown stencil coefficients k_i (i = 1, 2, ..., 27 with $k_{14} = 1$), and $q_{1,j}$, $q_{2,j}$ (j = 1, 2, ..., 25) in order to minimize the local truncation error. First, we zero the first 32 coefficients b_p in Eq. (16) up to the third order with respect to h; i.e.,

$$b_p = 0, p = 1, 2, ..., 32.$$
 (21)

Then, in order to have a sufficient number of equations for the calculation of the 76 unknown stencil coefficients k_i (i = i = 1, 2, ..., 27) and q_{1j} , q_{2j} (j = 1, 2, ..., 25), we use the least square method for the minimization of coefficients b_p related to the fourth, fifth and sixth orders of the local truncation error with the following residual R:

$$R = \sum_{p=33}^{50} b_p^2 + h_1 \sum_{p=51}^{72} b_p^2 + h_2 \sum_{p=73}^{98} b_p^2,$$
 (22)

where h_1 and h_2 are the weighting factors to be selected (e.g., the numerical experiments show that $h_1 = h_2 = 0.1$ yields accurate results). In order to minimize the residual R with the constraints given by Eq. (21), we can form a new residual \overline{R} with the Lagrange multipliers λ_l :

$$\overline{R} = \sum_{l=1}^{32} \lambda_l b_l + \sum_{p=33}^{50} b_p^2 + h_1 \sum_{p=51}^{72} b_p^2 + h_2 \sum_{p=73}^{98} b_p^2.$$
 (23)

The residual \overline{R} is a quadratic function of the stencil coefficients k_i (i=1,2,...,27) and $q_{1,j}, q_{2,j}$ (j=1,2,...,25) and a linear function of the Lagrange multipliers λ_i ; i.e., $\overline{R}=\overline{R}(k_i,q_{1,j},q_{2,j},\lambda_l)$. In order minimize the residual $\overline{R}=\overline{R}(k_i,q_{1,j},q_{2,j},\lambda_l)$, the following equations based on the least square method for the residual \overline{R} can be written down:

$$\frac{\partial \overline{R}}{\partial k_i} = 0, \qquad \frac{\partial \overline{R}}{\partial q_{1,j}} = 0, \qquad \frac{\partial \overline{R}}{\partial q_{2,j}} = 0, \qquad \frac{\partial \overline{R}}{\partial \lambda_l} = 0,
i = 1, 2, \dots, 27, \qquad i = 1, 2, \dots, 25, \qquad l = 1, 2, \dots, 32,$$
(24)

where equation $\frac{\partial \overline{R}}{\partial k_{14}} = 0$ in Eq. (24) should be replaced by $k_{14} = 1$; see Remark 3. Eq. (24) forms a system of 109 linear algebraic equations with

respect to 77 coefficients k_i (i = 1, 2, ..., 27) and $q_{1,i}, q_{2,i}$ (j = 1, 2, ..., 25) as well as 32 Lagrange multipliers λ_l (l=1,2,...,32). Solving these linear algebraic equations numerically, we can find the coefficients k_i (i = 1, 2,, 27) for the 27-point uniform stencils as well as $q_{1,j}$, $q_{2,j}$ (j=1,2,..., 25). As can be seen from Eq. (16), the presented procedure provides the fourth order of the local truncation error for the 27-point uniform stencils with the general geometry of the interface. The 27-point uniform stencils of OLTEM for a homogeneous material (without interface) provide the sixth order of the local truncation error for rectangular meshes; see Eq. (20). In this case the global error is defined by the order of accuracy of the 27-point stencils with interfaces. This leads to the third order of accuracy of global solutions; see the numerical examples below. Moreover, due to the minimization of the leading high-order terms b_p of the local truncation error in Eq. (23), at the same numbers of degrees of freedom the new approach on irregular interfaces yields more accurate results than those obtained by high-order finite elements (up to the sixth order) with much wider stencils; see the numerical examples below.

Remark 4. We should mention that the representation of the coefficients b_i in Eq. (16) as $b_i = \sum_{j=1}^{27} s_{ij} k_j + \sum_{j=1}^{25} (c_{ij}^1 q_{1,j} + c_{ij}^2 q_{2,j})$, $i=1,2,\ldots,98$ as well as the explicit analytical formulas for $\frac{\partial \overline{R}}{\partial k_i}$, $\frac{\partial \overline{R}}{\partial q_{1,j}}$, $\frac{\partial \overline{R}}{\partial q_2}$, $\frac{\partial \overline{R}}{\partial k_i}$ (see Eq. (24)) in terms of the coefficients s_{ij} , c_{ij}^1 and c_{ij}^2 (see Appendix B) significantly simplify the derivations and allowed us to extend our approach to the 3-D case.

The global discrete system of equations includes the 27-point stencils for homogeneous materials without interfaces and the 27-point stencils for heterogeneous materials with interfaces between different materials (see Fig. 1) for all internal grid points located inside the domain. The

Remark 6. It is interesting to mention that the stencil coefficients can be also derived using the Taylor series expansion about the central grid point with the coordinates x_{14} , y_{14} and z_{14} instead of the interface point with the coordinates x_G , y_G and z_G .

2.2. Nonzero source term $f_l \neq 0$ in Eq. (1)

The inclusion of non-zero source term f_l in the partial differential equation, Eq. (1), leads to the non-zero term \bar{f} in the stencil equation, Eq. (9) (similar to Eq. (3)). As we mentioned after Eq. (2), the functions f_l can be discontinuous across the interfaces. The expression for the term \bar{f} can be calculated from the procedure used for the derivation of the local truncation error in the case of zero source term as follows. In the case of non-zero source term $f_l(x) \neq 0$ and $\bar{f} \neq 0$, the insertion of Eqs. (12)–(15) into Eq. (11) yields the following local truncation error in space e_f :

$$e_{f} = e - \left[\overline{f} - \mathbf{h}^{2} \left\{ \sum_{j=1}^{27} \frac{1}{2} \left(r_{xj} - dx_{G} \right) \left(a_{j} \widetilde{f}_{G}^{*} + \left(1 - a_{j} \right) \widetilde{f}_{G}^{**} \right) k_{j} \right.$$

$$+ \left. \sum_{j=1}^{25} \left[\frac{1}{2} d_{x,j}^{2} (\widetilde{f}_{G}^{*} - \widetilde{f}_{G}^{**}) q_{1,j} + d_{x,j} n_{x,j} \left(e_{*} \widetilde{f}_{G}^{*} - e_{**} \widetilde{f}_{G}^{**} \right) q_{2,j} \right) \right] \right\} - \mathbf{h}^{3} \dots \right],$$

$$(25)$$

where e is the local truncation error in space given by Eq. (16) for zero source term, \widetilde{f}_G^* and \widetilde{f}_G^{**} designate functions $\frac{f^*(x,y,z)}{e_*}$ and $\frac{f^{**}(x,y,z)}{e_*}$ calculated at the interface point with the coordinates $x=x_G$, $y=y_G$ and $z=z_G$. Equating to zero the expression in the square brackets in the right-hand side of Eq. (25), we will get the expression for \overline{f} :

$$\overline{f} = \sum_{j=1}^{27} \widehat{f}_{j}^{1} k_{j} + \sum_{j=1}^{25} \left(\widehat{f}_{j}^{2} q_{1,j} + \widehat{f}_{j}^{3} q_{2,j} \right)
= \mathbf{h}^{2} \left\{ \sum_{j=1}^{27} \frac{1}{2} \left(r_{x,j} - dx_{G} \right) \left(a_{j} \widetilde{f}_{G}^{*} + \left(1 - a_{j} \right) \widetilde{f}_{G}^{**} \right) k_{j} + \sum_{j=1}^{25} \left[\frac{1}{2} d_{x,j}^{2} (\widetilde{f}_{G}^{*} - \widetilde{f}_{G}^{**}) q_{1,j} + d_{x,j} n_{x,j} \left(e_{x} \widetilde{f}_{G}^{*} - e_{**} \widetilde{f}_{G}^{**} \right) q_{2,j} \right) \right] \right\} + \mathbf{h}^{3} \dots,$$
(26)

new approach does not use unknowns at the interfaces and the global discrete system of equations has the same unknowns for homogeneous and heterogeneous materials (the same structures of the sparse global matrices, the difference is only in the values of the stencil coefficients k_p (see Eq. (9)) of the global matrices for homogeneous and heterogeneous materials).

Remark 5. To estimate the computation costs of the formation and solution of 109 linear algebraic equations given by Eq. (24) we formed and solved 10⁴ such systems with a general MATLAB solver on a desktop computer (Processor: Intel (R) Core(TN) i9-9900 CPU @3.10Hz 3.10 HZ). The computation 'wall' time was T = 49.89s for 10^4 systems or the average time for one system was 0.004989s. Because the coefficients k_p are independently calculated for different stencils, the computation time of their calculation for different stencils can be significantly reduced on modern parallel computers. These local systems are solved only for the grid points located close to the interface (for heterogeneous stencils). This means that for large global systems of equations, the computation time for the calculation of the coefficients k_p is very small compared to that for the solution of the global system of algebraic equations. We should mention that the coefficients $q_{1,j}$, $q_{2,j}$ calculated from the local system of equations, Eq. (24), are only used for the calculation of nonzero right-hand side vector (see below Section 2.2) while the Lagrange multipliers λ_l in the local system of equations, Eq. (24), are not used in the global system of equations at all.

as well as we will get the same local truncation errors $e_f=e$ for zero and non-zero source term. The coefficients \hat{f}_j^1 (j=1,2,...,27), \hat{f}_j^2 and \hat{f}_j^3 (j=1,2,...,25) in Eq. (26) are:

$$\widehat{f}_{j}^{1} = \mathbf{h}^{2} \left(\frac{1}{2} \left(r_{x,j} - dx_{G} \right) \left(a_{j} \widetilde{f}_{G}^{*} + \left(1 - a_{j} \right) \widetilde{f}_{G}^{**} \right) + \mathbf{h}^{3} \dots,$$

$$\widehat{f}_{j}^{2} = \mathbf{h}^{2} \left(\frac{1}{2} d_{x,j}^{2} \widetilde{f}_{G}^{*} - \widetilde{f}_{G}^{**} \right) + \mathbf{h}^{3} \dots,$$

$$\widehat{f}_{j}^{3} = \mathbf{h}^{2} d_{x,j} n_{x,j} \left(e_{x} \widetilde{f}_{G}^{*} - e_{x,x} \widetilde{f}_{G}^{**} \right) + \mathbf{h}^{3} \dots,$$
(27)

see the attached file 'RHS.nb' for the detailed expressions of \hat{f}_j^1 , \hat{f}_j^2 and \hat{f}_j^3 . This means that the coefficients k_i (i=1,2,...,27) of the stencil equations are first calculated for zero source term $f_l=0$ as described in Section 2.1. Then, the nonzero source term \bar{f} given by Eq. (26) is used in the stencil equation, Eq. (9).

3. OLTEM for post-processing of numerical results - calculations of spatial derivatives

For the analysis of engineering problems the calculations of the spatial derivatives of primary functions are necessary in many cases; e. g., the spatial derivatives of function u_l in Eq. (1). Therefore, after the calculation of the numerical solution for the primary functions, many computer codes include special post-processing procedures for the

calculation of the spatial derivatives of the numerical solution for the primary functions. Here we show the application of OLTEM with the compact 27-point stencils (the same as we used in the previous section; see also Fig. 1) for the calculation of $\frac{\partial u_i^{num}}{\partial x}$, $\frac{\partial u_i^{num}}{\partial y}$ and $\frac{\partial u_i^{num}}{\partial z}$. Because the calculations of these three derivatives are similar then we show the procedure in detail for $\frac{\partial u_i^{num}}{\partial x}$.

The compact 27-point stencils for the calculation of $\frac{\partial u^{min}}{\partial x}$ at the central stencil point with the coordinates x_{14} , y_{14} and z_{14} (see Fig. 1) can be selected similar to Eq. (9) as follows:

$$-\left[a_{14}\frac{\partial u_{14}^{*,num}}{\partial x} + (1 - a_{14})\frac{\partial u_{14}^{**,num}}{\partial x}\right]h + \sum_{p=1}^{27} k_p \left[a_p u_p^{*,num} + (1 - a_p)u_p^{**,num}\right] = \overline{f},$$
(28)

where $a_{14}=1$ if the central stencil point belongs to material * and $a_{14}=0$ if the central stencil point belongs to material **. The local truncation error e_p for Eq. (28) can be obtained by the replacement of the numerical solution $u_p^{*,num}$ and $u_p^{**,num}$ in Eq. (28)by the exact solution u_p^* and u_p^{**} :

$$e_{p} = -\left[a_{14}\frac{\partial u_{14}^{*}}{\partial x} + (1 - a_{14})\frac{\partial u_{14}^{**}}{\partial x}\right]h + \sum_{p=1}^{27} k_{p}\left[a_{p}u_{p}^{*} + (1 - a_{p})u_{p}^{**}\right] - \overline{f}.$$
(29)

Similar to Eq. (11) in Section 2, we include the interface conditions for the exact solution at the same small number N_G of the interface points in the expression for the local truncation error in Eq. (29) as follows:

$$\begin{split} e_{p} &= -\left[a_{14}\frac{\partial u_{14}^{*}}{\partial x} + (1 - a_{14})\frac{\partial u_{14}^{**}}{\partial x}\right]h + \sum_{p=1}^{27}k_{p}\left[a_{p}u_{p}^{*} + (1 - a_{p})u_{p}^{**}\right] \\ &+ \left\{\sum_{j=1}^{N_{G}}q_{1,j}\left(u_{G,j}^{*} - u_{G,j}^{**}\right) + \sum_{j=1}^{N_{G}}hq_{2,j}\left[e_{*}\left(n_{x,j}\frac{\partial u_{G,j}^{*}}{\partial x} + n_{y,j}\frac{\partial u_{G,j}^{*}}{\partial y} + n_{z,j}\frac{\partial u_{G,j}^{*}}{\partial z}\right)\right. \\ &- \left. e_{**}\left(n_{x,j}\frac{\partial u_{G,j}^{**}}{\partial x} + n_{y,j}\frac{\partial u_{G,j}^{**}}{\partial y} + n_{z,j}\frac{\partial u_{G,j}^{**}}{\partial z}\right)\right]\right\} - \overline{f}, \end{split}$$

$$(30)$$

see the corresponding explanations in Section 2.1. Similar to Section 2, first we consider the case of zero source term $f_l = \overline{f} = 0$. For the accurate calculation of the derivative $\frac{\partial u^{num}}{\partial x}$, we should minimize the local truncation error e_p in Eq. (30). Repeating the procedure described in Section 2.1 and using Eqs. (12) - (15) with zero source term $f^* = f^{**} = 0$ we will get the following local truncation error in space e_p :

$$e_{p} = b_{1}u_{G}^{2} + b_{2}u_{G}^{*}$$

$$+h\left(b_{3}\frac{\partial u_{G}^{*}}{\partial z} + b_{4}\frac{\partial u_{G}^{**}}{\partial z} + b_{5}\frac{\partial u_{G}^{*}}{\partial y} + b_{6}\frac{\partial u_{G}^{**}}{\partial y} + b_{7}\frac{\partial u_{G}^{*}}{\partial x} + b_{8}\frac{\partial u_{G}^{**}}{\partial x}\right) + h^{2}\left(b_{9}\frac{\partial^{2}u_{G}^{*}}{\partial z^{2}} + b_{10}\frac{\partial^{2}u_{G}^{**}}{\partial z^{2}} + b_{11}\frac{\partial^{3}u_{G}^{*}}{\partial z\partial y^{2}} + b_{12}\frac{\partial^{3}u_{G}^{**}}{\partial z\partial y^{2}} + b_{13}\frac{\partial^{2}u_{G}^{*}}{\partial y^{2}} + b_{14}\frac{\partial^{2}u_{G}^{**}}{\partial y^{2}} + b_{15}\frac{\partial^{3}u_{G}^{*}}{\partial z\partial x^{2}} + b_{16}\frac{\partial^{3}u_{G}^{*}}{\partial z\partial x^{2}} + b_{17}\frac{\partial^{2}u_{G}^{*}}{\partial x\partial y} + b_{18}\frac{\partial^{2}u_{G}^{**}}{\partial x\partial y}\right) + \dots$$
(31)

where similar to Eq. (16) the coefficients b_p (p=1,2,...) are expressed in terms of the coefficients k_i and $q_{1,j}$, $q_{2,j}$ (i=1,2,...,27, $j=1,2,...,N_G$) and are given in the file 'b-coef-post.nb'.

For homogeneous materials (without interfaces), the coefficients $q_{1j}=0$ $q_{2j}=0$ $(j=1,2,...,N_G)$ are zero and the stencils coefficients k_i (i=1,2,...,27) can be analytically found similar to those in Section 2.1.1. In this case we use the following system of 27 algebraic equations:

$$b_p = 0, p = 1, 3, 5, 7, 9, 11, 13, 15, 17, 19, 21, 23, 25, 27, 29, 31, 33, 35, 37, 41, 45, 47, 53, 55, 67, 73, 77$$
 (32)

where in contrast to Eqs. (17) and (18) from Section 2.1.1, here we replace Eq. (18) by equation $b_{73}=0$. The solution of Eq. (32) yields the

stencil coefficients given in Appendix D. These coefficients yields the following local truncation error e_p :

$$e_p = \frac{h^5}{360} \left[(7 - 5b_z^2) \frac{\partial^5 u_{14}}{\partial x \partial z^4} + \left(7 - 5b_y^2 \right) \frac{\partial^5 u_{14}}{\partial x \partial v^4} \right] + O(h^{10}). \tag{33}$$

For heterogeneous materials with interfaces, the stencil coefficients k_i and $q_{1,j}$, $q_{2,j}$ (i=1,2,...,27, $j=1,2,...,N_G$) are calculated similar to those in Section 2.1.2 from 109 linear algebraic equations formed by Eq. (24). In contrast to Section 2.1.2, in Eq. (24) we do not replace equation $\frac{\partial \overline{R}}{\partial k_{14}} = 0$ by $k_{14} = 1$. Due to Eq. (21), the stencil coefficients for heterogeneous materials provide the 4th order of accuracy for the local truncation error e_0 .

The case of zero source term $f_l \neq 0$ is treated similar to that in Section 2.2. The final expression for the term \bar{f} in Eq. (28) is also described by Eq. (26); see the attached file 'RHS-post.nb' for the detailed expressions of \hat{f}_{i}^1 , \hat{f}_{i}^2 and \hat{f}_{i}^3 .

To summarize, for the calculation of the derivative $\frac{\partial u^{num}}{\partial x}$ using OLTEM with the 27-point stencils, we should follow the following procedure:

- Calculate the stencil coefficients k_i and $q_{1,j}$, $q_{2,j}$ ($i=1,2,...,27, j=1,2,...,N_G$) for each internal grid point as described above in Section 3 for homogeneous (without interfaces) and heterogeneous (with interfaces) materials.
- Using these stencil coefficients, calculate the right-hand side \bar{f} in Eq. (28) for each internal grid point using Eq. (26).
- Calculate the derivative $\frac{\partial u^{num}}{\partial x}$ from Eq. (28) for each internal grid point as follow:

$$\frac{\partial u_{14}^{*,num}}{\partial x} = \frac{1}{h} \left[\sum_{p=1}^{27} k_p \left[a_p u_p^{*,num} + (1 - a_p) u_p^{**,num} \right] - \overline{f} \right], \tag{34}$$

if the central stencil point belongs to material * ($a_{14} = 1$) and

$$\frac{\partial u_{14}^{**,num}}{\partial x} = \frac{1}{h} \left[\sum_{p=1}^{27} k_p \left[a_p u_p^{*,num} + (1 - a_p) u_p^{**,num} \right] - \overline{f} \right], \tag{35}$$

if the central stencil point belongs to material ** $(a_{14} = 0)$.

The calculation of the derivatives $\frac{\partial u^{num}}{\partial y}$ and $\frac{\partial u^{num}}{\partial z}$ can be done similar to the calculation of the derivative $\frac{\partial u^{num}}{\partial x}$ as described above.

Remark 7. If any of the grid points included into the stencil is located on the boundary with the Dirichlet boundary conditions then for this point p in Eqs. (34) and (35) we use the exact value of $u_p^{*,num}$ or $u_p^{**,num}$ defined by the boundary conditions. In the case of the Neumann boundary conditions, the procedure can be modified similar to that in our paper [39] for OLTEM with irregular boundaries and the Neumann boundary conditions.

It is interesting to note that for homogeneous materials the post-processing procedure described above can be also used for the calculation of the spatial derivatives without the application of the partial differential equation as in other post-processing techniques (e.g., see [36–38] for finite and isogeometric elements). Let us assume that we can calculate the derivative $\frac{\partial u^{num}}{\partial x}$ at the internal grid point in terms of the values of the function u^{num} at the neighboring grid points. For simplicity, we will use a uniform Cartesian mesh and 27 grid points for the calculation of the derivative $\frac{\partial u^{num}}{\partial x}$ at the central grid point (see Fig. 1a) as follows:

$$-h\frac{\partial u_{14}^{num}}{\partial x} + \sum_{p=1}^{27} k_p u_p^{num} = 0$$
 (36)

with the following local truncation error:

$$e_p = -h \frac{\partial u_{14}}{\partial x} - \sum_{p=1}^{27} k_p u_p.$$
 (37)

Repeating the procedure described in Section 2.1 without the use of Eqs. (14) and (15) and zeroing the corresponding coefficients b_p in the Taylor expansion of the local truncation error e_p , we can show that $k_{15} = 1/2$ and $k_{13} = -1/2$ (all other $k_i = 0$, i = 1, 2, ..., 12, 14, 16, 17, ..., 27) in Eq. (36) yield the optimal order of e_p in Eq. (37):

$$e_p = -\frac{h^3}{6} \frac{\partial^3 u_{14}}{\partial x^3} + O(h^4). \tag{38}$$

In this case we have the well-known finite-difference approximation of the derivative. Comparing Eqs. (38) and (33) we can see that the use of PDE for post-processing improves the accuracy of the spatial derivative by two orders for the same 27-point compact stencils. We should also mention that the approximation given by Eq. (36) cannot be used for the stencils with interfaces (as those in Fig. 1b).

To summarize, the proposed post-processing procedure provides the optimal accuracy of the spatial derivatives of primary functions calculated with the help of compact stencils. It can be developed with or without the use of PDEs. However, the use of PDEs significantly improves the accuracy of the spatial derivatives for the given stencils.

Despite the fact that we have applied the proposed post-processing technique to the stencils defined on Cartesian meshes, it can be also used for non-uniform meshes with the corresponding coefficients r_{xp} , r_{yp} , r_{zp} in Eq. (6) (similar to OLTEM developed in our papers [27,29,39] for irregular boundaries). Finally, the post-processing procedure developed can be independently used with any known numerical technique (e.g., with finite elements).

4. Numerical examples

In this section the computational efficiency of OLTEM with the 27-point stencils developed for the solution of the 3-D Poisson equation with discontinuous coefficients will be demonstrated and compared with conventional linear and high order (up to 7th order, the highest order in 'COMSOL') tetrahedral finite elements. For finite element calculations, the commercial finite element software 'COMSOL' with isoparametric finite elements is used. In order to compare the accuracy of OLTEM with FEM, the following errors are considered below. The relative error e^i_w for the function w at the jth grid point is defined as:

$$e_{w}^{j} = \frac{\left| w_{j}^{num} - w_{j}^{exact} \right|}{w_{\max}^{exact}}, \qquad j = 1, 2, ..., N.$$
 (39)

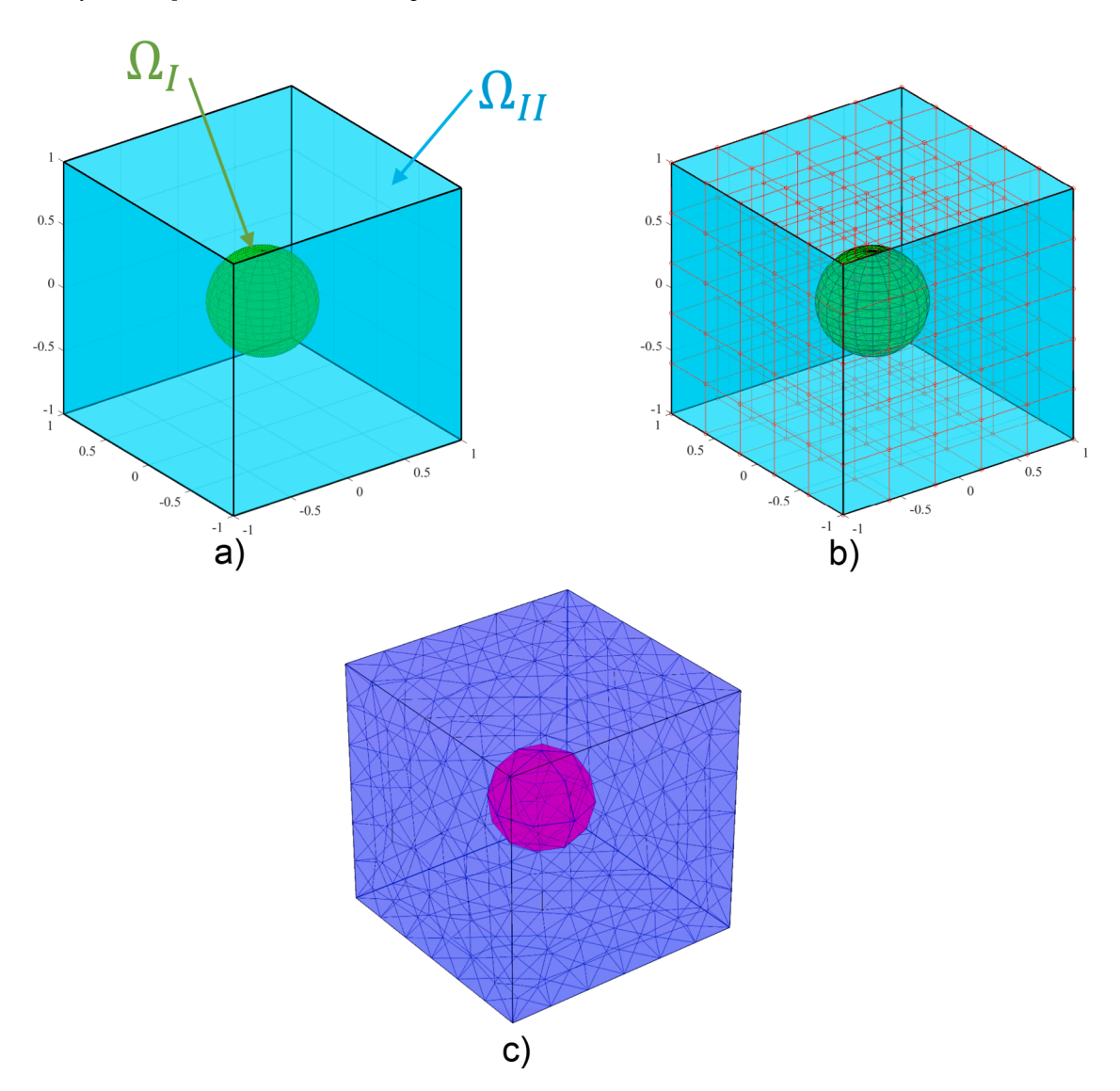
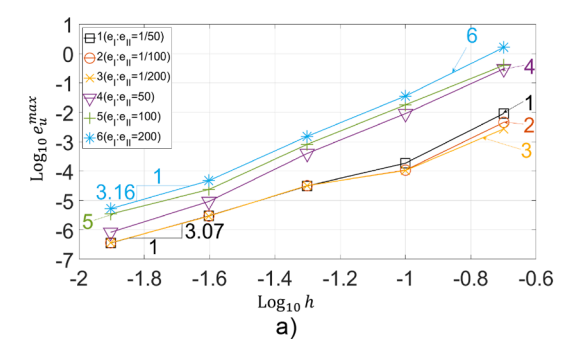


Fig. 2. A 3-D cube with a spherical inclusion (a), the examples of an unfitted Cartesian mesh for OLTEM (b) and a conformed tetrahedral finite element mesh generated by the commercial software COMSOL (c).



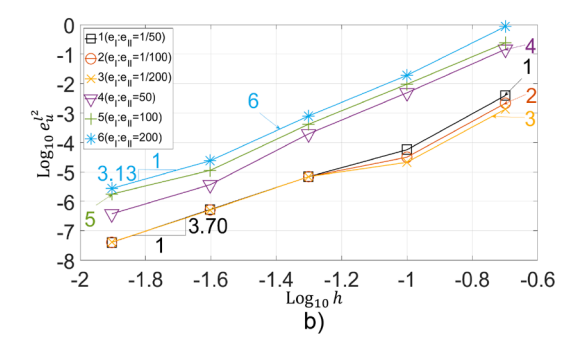


Fig. 3. The maximum relative error e_u^{\max} (a) and the l^2 error norm $e_u^{l^2}$ (b) as a function of the mesh size h at mesh refinement in the logarithmic scale. The numerical solutions of the 3-D Poisson equation for the cube with the spherical inclusion (see Fig. 2a) are obtained by OLTEM on square ($b_y = 1$ and $b_z = 1$) Cartesian meshes with the following material contrasts: $\frac{e_l}{e_{ll}} = \frac{1}{50}$ (curve 1), $\frac{e_l}{e_{ll}} = \frac{1}{100}$ (curve 2), $\frac{e_l}{e_{ll}} = \frac{1}{200}$ (curve 3), $\frac{e_l}{e_{ll}} = 50$ (curve 4), $\frac{e_l}{e_{ll}} = 100$ (curve 5) and $\frac{e_l}{e_{ll}} = 200$ (curve 6).

The maximum relative error e_w^{max} for the function w is defined as:

$$e_w^{\max} = \max_j e_w^j, \qquad j = 1, 2, ..., N.$$
 (40)

In Eqs. (39)-(40) the superscripts 'num' and 'exact' correspond to the numerical and exact solutions, N is the total number of the grid points used in calculations, w_{\max}^{exact} is the maximum absolute value of the exact solution over the entire domain for the function w. We also use the L^2 error norm for finite elements (e.g., see [40]) and the l^2 error norm (e.g., see [41]) for OLTEM:

$$e_{w}^{l^{2}} = \left\{ dx dy dz \sum_{i=0}^{N_{x}} \sum_{j=0}^{N_{y}} \sum_{k=0}^{N_{k}} \left[w^{num} \left(x_{i}, y_{j}, z_{k} \right) - w^{exact} \left(x_{i}, y_{j}, z_{k} \right) \right]^{2} \right\}^{\frac{1}{2}} / \left| w^{exact} \right|_{L^{2}},$$
(41)

where N_x , N_y and N_k are the numbers of Cartesian grid points along x, y and z-axes, x_i , y_j and z_k are the coordinates of Cartesian grid points, respectively. As function w in Eqs. (39)–(41) we consider u, $\frac{\partial u}{\partial x}$, $\frac{\partial u}{\partial y}$ and $\frac{\partial u}{\partial z}$.

4.1. 3-D Bi-material cube with a spherical inclusion

Let us consider the 3-D Poisson equation with discontinuous coefficients for the bi-material cube with dimensions $2 \times 2 \times 2$ as shown in Fig. 2a. The cube consists of a spherical inclusion (subdomain Ω_I) at the center of the cube and the matrix (subdomain Ω_{II}) with the circular interface described by the following equation:

$$x^2 + y^2 + z^2 = r^2, (42)$$

where r=0.4 is the radius of the circular interface. The following material properties are assumed: $e_I = \frac{1}{50}$; $\frac{1}{100}$; $\frac{1}{200}$; 50; 100; 200 in Ω_I and e_{II}

= 1 in Ω_{II} with the material contrasts $\frac{e_I}{e_{II}} = \frac{1}{50}$; $\frac{1}{100}$; $\frac{1}{200}$; 50; 100; 200. Using the method of manufactured solution, the following exact solution to the Poisson equation is selected:

$$u(x, y, z) = \begin{cases} \cos\left(\frac{x^2}{r^2} + \frac{y^2}{r^2} + \frac{z^2}{r^2}\right) & \text{in } \Omega_I \\ \frac{e_I}{e_{II}}\cos\left(\frac{x^2}{r^2} + \frac{y^2}{r^2} + \frac{z^2}{r^2}\right) - \left(\frac{e_I}{e_{II}} - 1\right)\cos(1) & \text{in } \Omega_{II} \end{cases}$$
(43)

This solution meets the interface conditions, Eq. (2). The source terms can be calculated by the substitution of the exact solution into the Poisson equation, Eq. (1), and are given below:

$$\begin{split} f_I(x,y,z) &= -2e_I \left[\frac{2}{r^2} \left(\frac{x^2}{r^2} + \frac{y^2}{r^2} + \frac{z^2}{r^2} \right) \cos \left(\frac{x^2}{r^2} + \frac{y^2}{r^2} + \frac{z^2}{r^2} \right) + \left(\frac{3}{r^2} \right) \sin \left(\frac{x^2}{r^2} + \frac{y^2}{r^2} + \frac{z^2}{r^2} \right) \right] \\ &\text{in} \quad \Omega_I \\ f_{II}(x,y,z) &= -2e_I \left[\frac{2}{r^2} \left(\frac{x^2}{r^2} + \frac{y^2}{r^2} + \frac{z^2}{r^2} \right) \cos \left(\frac{x^2}{r^2} + \frac{y^2}{r^2} + \frac{z^2}{r^2} \right) + \left(\frac{3}{r^2} \right) \sin \left(\frac{x^2}{r^2} + \frac{y^2}{r^2} + \frac{z^2}{r^2} \right) \right] \end{split}$$

The Dirichlet boundary conditions along all faces of the cube are imposed according to the exact solution, Eq. (43). The problem is solved by OLTEM with the 27-point stencils as well as by linear and high order (up to the 7th order) finite elements for different material contrasts $\frac{e_I}{e_{BI}}$. Figure 2b,c shows a typical unfitted Cartesian mesh with aspects ratios $b_y = b_z = 1$ used for OLTEM as well as a typical conformed tetrahedral finite element mesh.

First, we present the application of OLTEM to the solution of the Poisson equation for heterogeneous materials with different material contrasts $\frac{e_l}{e_l}$. Figure 3 shows the maximum error e_u^{\max} and the l^2 error norm $e_u^{l^2}$ as a function of the mesh size h in the logarithmic scale for OLTEM with the 27-point stencils and the material contrasts $\frac{e_l}{e_l}$

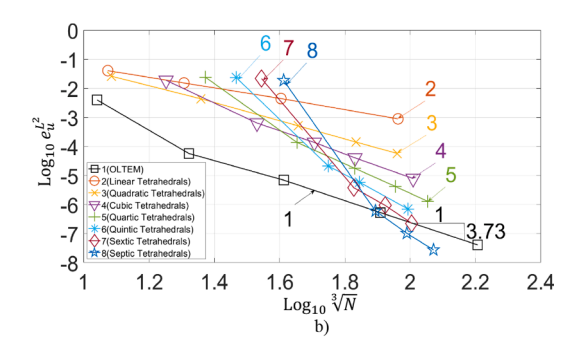


Fig. 4. The maximum relative error e_u^{\max} (a) and the L^2 error norm $e_u^{L^2}$ (b) as a function of $\sqrt[3]{N}$ at mesh refinement in the logarithmic scale (N is the number of degrees of freedom). The numerical solutions of the 3-D Poisson equation for the cube with the spherical inclusion and the material contrast $\frac{e_L}{e_H} = \frac{1}{50}$ (see Fig. 2a) are obtained by OLTEM on square ($b_y = 1$ and $b_z = 1$) Cartesian meshes (curve 1) as well as by linear and high-order tetrahedral finite elements (curves 2 - 8). Curves 2, 3, ...,8 correspond to linear, quadratic,..., and the 7th order elements.

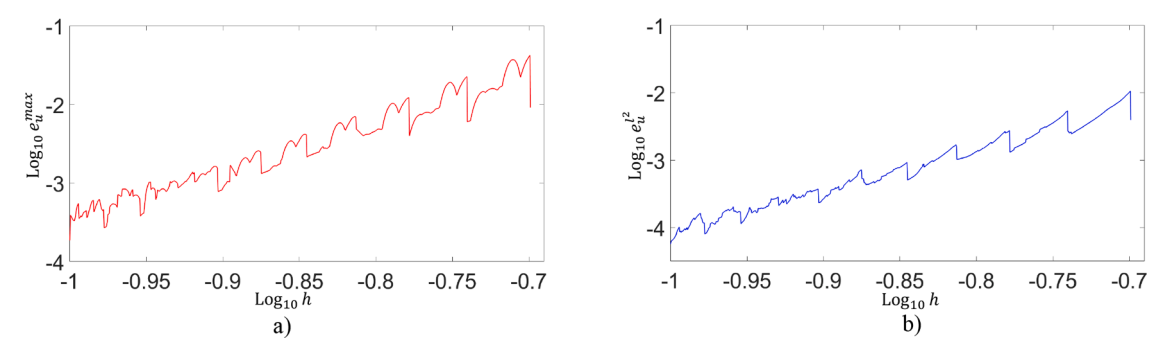


Fig. 5. The logarithm of the maximum relative errors e_u^{max} (a) and the l^2 error norm $e_u^{l^2}$ (b) as a function of the mesh size h. The numerical solutions of the 3-D Poisson equation for the cube with the spherical inclusion (see Fig. 2a) are obtained by OLTEM on square ($b_y = 1$ and $b_z = 1$) Cartesian meshes with the material contrast $\frac{e_l}{e_l} = \frac{1}{50}$. Each curve is calculated on 1001 meshes; see the text.

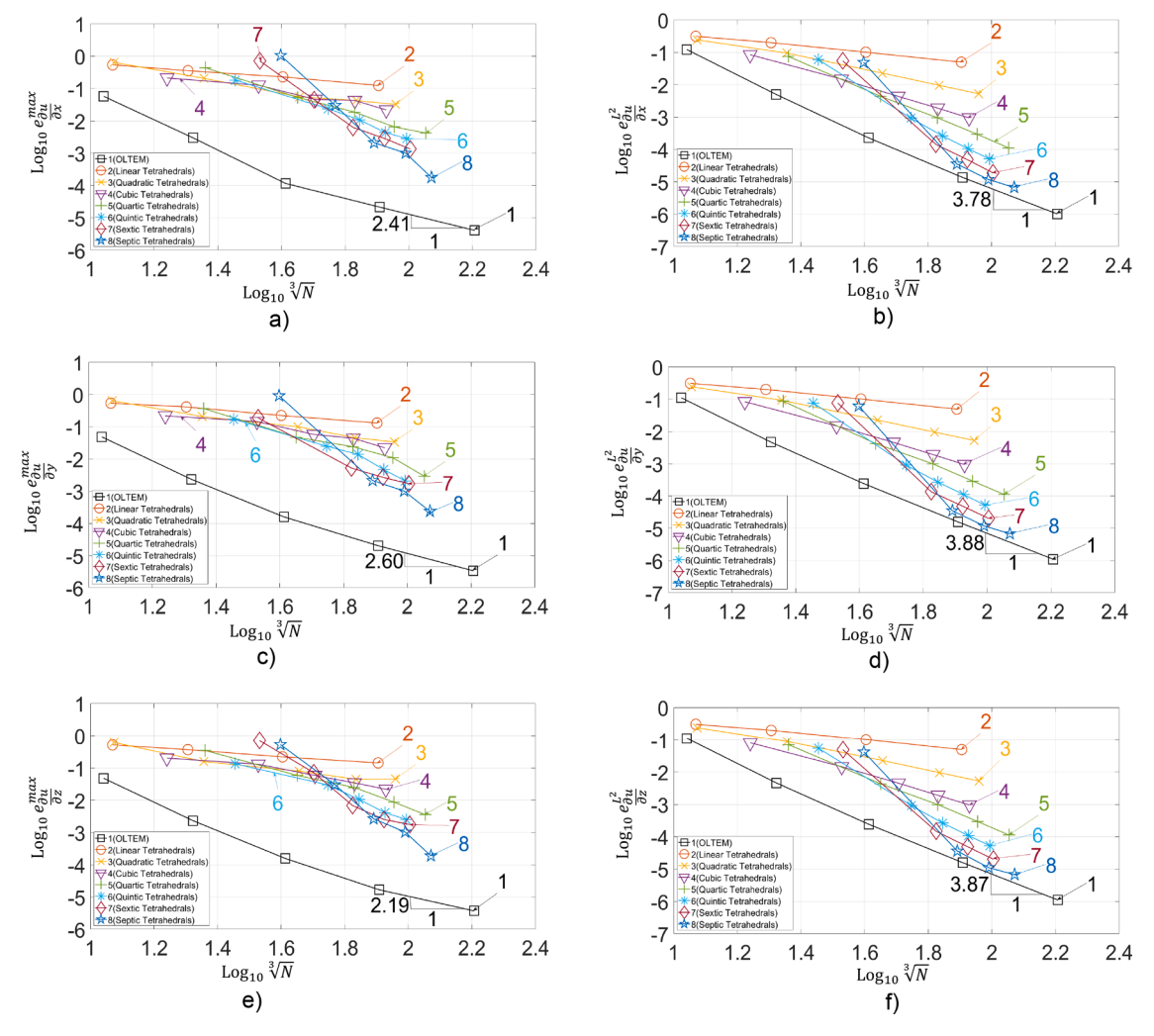


Fig. 6. The maximum relative errors $e_{\frac{m}{dz}}^{max}$ of the *x*-derivative of the function u (a), $e_{\frac{m}{dy}}^{max}$ of the *y*-derivative of the function u (c) and $e_{\frac{m}{dz}}^{max}$ of the *z*-derivative of the function u (e) as well as the L^2 error norm $e_{\frac{d}{dz}}^{L^2}$ of the *x*-derivative of the function u (b), $e_{\frac{d}{dy}}^{L^2}$ of the *y*-derivative of the function u (d), and $e_{\frac{d}{dz}}^{max}$ of the *z*-derivative of the function u (f) as a function of $\sqrt[3]{N}$ at mesh refinement in the logarithmic scale (*N* is the number of degrees of freedom). The numerical solutions of the 3-D Poisson equation for the cube with the spherical inclusion and the material contrast $\frac{e_1}{e_1} = \frac{1}{50}$ (see Fig. 2a) are obtained by OLTEM on square ($b_y = 1$ and $b_z = 1$) Cartesian meshes (curve 1) as well as by linear and high-order tetrahedral finite elements (curves 2–8). Curves 2, 3, ...,8 correspond to linear, quadratic,..., and the 7th order elements.

 $\frac{1}{50}$; $\frac{1}{100}$; $\frac{1}{200}$; 50; 100; 200. As can be seen from Fig. 3, OLTEM yields convergent results with the order of convergence close or greater than three for all material contrasts. These observations are in agreement

with the theoretical results in the previous Section 2.

Next, we present the accuracy comparison of OLTEM with linear and high order (up to the 7th order - the highest order in COMSOL) finite $\frac{1}{2}$

elements for the material contrast $\frac{e_I}{e_B} = \frac{1}{50}$ (similar results can be also obtained for other material contrasts). Figure 4 shows the maximum relative errors e_u^{max} and the errors $e_u^{L^2}$ in the L^2 norm as a function of the number N of degrees of freedom in the logarithmic scale for the numerical results obtained by OLTEM and by finite elements. As can be seen from Fig. 4, at the same N the numerical results obtained by OLTEM are much more accurate than those obtained by linear and higher order finite elements (up to the 7th order elements for the maximum relative errors e_u^{max} and up to the 6th order elements for the L^2 error norm $e_u^{L^2}$; see Fig. 4a,b). In addition to that, up to the accuracy of 0.0001% (-6 in the logarithmic scale along the y-axis in Fig. 4b) OLTEM yields more accurate results than those obtained by finite elements up to the 7th order. This increase in accuracy by OLTEM is impressive considering the fact that higher order finite elements have much wider stencils compared to those for OLTEM (the width of the stencils for OLTEM corresponds to that for linear finite elements) and require a much greater computation time. We should also mention that at the computational costs of linear finite elements, at the engineering accuracy of 0.1%, OLTEM reduces the number N of degrees of freedom by a factor of greater than 3500 for the maximum relative error $e_u^{\rm max}$ and greater than 250 for the L^2 error norm $e_u^{L^2}$ compared to that for linear finite elements; see Fig. 4a,b. This will lead to a huge reduction in the computation time for OLTEM compared to linear finite elements at a given accuracy.

The detailed study of the convergence and stability of the numerical results obtained by OLTEM is shown in Fig. 5. For this study, we solve the test problem with the material contrast $\frac{e_I}{e_{II}} = \frac{1}{50}$ on 1001 Cartesian meshes with the mesh sizes $h_i=\overline{h}_1+rac{(\overline{h}_2-\overline{h}_1)(i-1)}{1000}$ and a very small variation of the mesh size h where $\overline{h}_1 = 1/5 = 0.2$, $\overline{h}_2 = 1/10 = 0.1$ and i = 1, 2,...,1001. For these meshes, three grid planes always coincide with the left, bottom and rear faces of the cubical domain and at the small variation of the mesh size h we have very different locations of the circular interface with respect to the grid points. The curves in Fig. 5 correspond to curves 1 in Fig. 3. As can be seen from Fig. 5, the numerical results obtained by OLTEM on these meshes converge with the decrease in the grid size h. Small oscillations in Fig. 5 decrease with the decrease in the mesh size. This oscillatory behavior can be explained by the fact that at small variations of the mesh size h, there is a discontinuous change in the location of the grid points with respect to the interface (e.g., some grid points that belong to one material for the previous mesh can belong to another material for the next mesh; this leads to the discontinuous change of some stencils equations for the meshes with a small difference in h). It is important to mention that small oscillations in numerical convergence curves are typical for many numerical techniques at small variations of h. For example, the change in the angles of finite elements at small variations of the element size h also leads to such oscillations in convergence curves for finite element techniques.

The application of the new post-processing procedure for the calculation of the spatial derivatives of numerical solutions is presented in Fig. 6. Here, we solve the test problem with the material contrast $\frac{e_I}{e_I} = \frac{1}{50}$ by OLTEM as well as by linear and high order finite elements and compare the accuracy of the spatial derivatives $\frac{\partial u^{num}}{\partial x}$, $\frac{\partial u^{num}}{\partial y}$ and $\frac{\partial u^{num}}{\partial z}$ of the numerical solutions u^{num} . Figure 6 shows the maximum relative errors $e^{max}_{\frac{nu}{nx}}$, $e^{max}_{\frac{nu}{ny}}$, $e^{max}_{\frac{num}{nx}}$ and the errors $e^{L^2}_{\frac{nu}{nx}}$, $e^{L^2}_{\frac{nu}{ny}}$, $e^{L^2}_{\frac{nu}{nz}}$ in the L^2 norm as a function of the number N of degrees of freedom for different techniques. As can be seen from Fig. 6, at the same N the spatial derivatives $\frac{\partial u^{num}}{\partial x}$, $\frac{\partial u^{num}}{\partial y}$ and $\frac{\partial u^{num}}{\partial z}$ obtained by OLTEM are much more accurate than those obtained by linear and high-order (up to the 7th order) finite elements for the both selected error norms. The numerical results also show that the order of convergence of the spatial derivatives $\frac{\partial u^{num}}{\partial y}$, $\frac{\partial u^{num}}{\partial z}$ for the L^2 error norm is higher than that for the maximum relative error; compare the slopes of the curves in Fig. 6a,c,e with those in Fig. 6b,d,f. We should also mention that at the engineering accuracy of 0.1% for the spatial

derivatives, OLTEM reduces the number N of degrees of freedom by a factor of greater than 2.9×10^9 for the maximum relative error and greater than 1.15×10^6 for the L^2 error norm compared to that for linear finite elements; see Fig. 6). In order to find the intersection of curves 2 in Fig. 6 with the horizontal lines -3 along the vertical axis (for the accuracy of 0.1%) and to estimate this reduction in N, we extrapolated the curves 2 using the constant slope. Due to the new post-processing procedure, OLTEM is even more efficient for the calculation of the spatial derivatives $\frac{\partial u^{num}}{\partial x}$, $\frac{\partial u^{num}}{\partial y}$ and $\frac{\partial u^{num}}{\partial z}$ compared to linear and high order finite elements. This will lead to a huge reduction in the computation time for the calculation of the spatial derivatives by OLTEM compared to those obtained by finite elements at a given accuracy.

5. Concluding remarks

OLTEM developed in our paper [35] for the 2-D Poisson equation with heterogeneous materials is here extended to the general 3-D case. 27-point stencils (similar to those for linear finite elements) and unfitted Cartesian meshes for irregular geometry are used. One of the main ideas of the proposed approach for heterogeneous materials with interfaces is the addition of the interface conditions at a small number of interface points to the expression for the local truncation error. The unknown stencil coefficients are numerically calculated from a small local system of algebraic equations for the general geometry of interfaces. OLTEM does not change the width of the stencil equations; i.e., the size of the global discrete system of equations is the same for the Poisson equation with constant or discontinuous coefficients. The calculation of the unknown stencil coefficients is based on the minimization of the local truncation error of the stencil equations and yields the optimal order of accuracy of the new technique at a given stencil width. The increase in the computational costs for the calculation of the unknown stencil coefficients from the local system is insignificant compared to the computational costs for the solution of the global discrete system. Another novelty of the paper is the development of a new post-processing procedure for the accurate calculations of the spatial derivatives of numerical solutions. We show that OLTEM with compact stencils can significantly improve the accuracy of the spatial derivatives of numerical solutions as well. The proposed post-processing includes the use of the partial differential equations and the solution of the local systems of algebraic equations similar to those used for the calculations of the stencils coefficients in the basic approach.

The main advantages of the suggested technique can be summarized as follows:

- Many difficulties of the existing numerical techniques for irregular domains (e.g., finite elements, spectral element, isogeometric elements, the finite volume method, and many other) are related to complicated mesh generators for conformed meshes and the accuracy of 'bad' elements (e.g., the elements with small angles). In contrast to these techniques, OLTEM is based on trivial unfitted Cartesian meshes with a trivial procedure for the formation of the 27point stencils for 3-D domains with complex irregular interfaces.
- The new approach has the same width of the stencil equations and
 the same structure of the sparse global discrete equations for the
 Poisson equation with constant and discontinuous coefficients. There
 are no unknowns on the interfaces between different materials for
 the proposed technique; i.e., complex irregular interfaces do not
 affect the structure of the global system of equations (they affect just
 the values of the stencils coefficients).
- In contrast to the finite-difference techniques with the stencil coefficients calculated through the approximation of separate partial derivatives, the entire partial differential equation is used for the calculation of the stencil coefficients in OLTEM. This leads to the optimal accuracy of the proposed technique. E.g., the 27-point stencils of the new 3-D approach provide the optimal accuracy that cannot be improved without changing the width of stencil equations. In contrast

to the 27-point stencils of linear quadrilateral finite elements, OLTEM yields a higher order of accuracy (by one order) compared to that for linear finite elements for the general geometry of interfaces.

- The numerical results for irregular interfaces also show that at the same number of degrees of freedom, OLTEM is even much more accurate than high-order (up to the sixth order) finite elements with much wider stencils. This also means that at a given accuracy, OLTEM significantly reduces the computation time compared to that for linear and high-order finite elements. For example, at accuracy of 0.1% OLTEM decreases the number of degrees of freedom by a factor of greater than 3500 compared to linear finite elements with similar stencils and conformed meshes.
- OLTEM does not require time consuming numerical integration for finding the coefficients of the stencil equations; e.g., as for high-order finite, spectral and isogeometric elements. The stencil coefficients are calculated analytically or numerically (for the general geometry of interfaces) by the solution of small local systems of linear algebraic equations. Numerical experiments show that the solution of these small local systems of algebraic equations is fast. Moreover, these local systems are independent of each other and can be efficiently solved on a parallel computer.
- It was shown that OLTEM with the 27-point compact stencils used for the basic computations can be also applied (with small modifications) to the calculation of the spatial derivatives of numerical solutions at post-processing. The proposed post-processing procedure includes the use of the partial differential equation and the solutions of the small local systems of equations. Numerical experiments show that OLTEM with 27-point stencils used for basic computations and post-processing yields much more accurate results for the spatial derivatives of the numerical solution than those obtained by linear and high-order (up to the 7th order) finite elements with much wider stencils. At the engineering accuracy of 0.1% for the spatial derivatives, OLTEM decreases the number of degrees of freedom by a factor of greater than 10⁶ compared to linear finite elements.
- The proposed post-processing procedure provides the optimal accuracy of the spatial derivatives of the numerical solution for the selected compact stencils. It can be developed with or without the use of PDEs. However, the use of PDEs significantly improves the accuracy of the spatial derivatives for the given stencils (e.g., by two

- orders for the same 27-point stencils). Despite the fact that we have applied OLTEM to the stencils defined on Cartesian meshes, the proposed post-processing technique can be equally used for non-uniform meshes (similar to OLTEM developed in our papers [27, 29,39] for irregular boundaries). Finally, the post-processing procedure developed can be independently used with any known numerical technique (e.g., with finite elements).
- Due to the huge reduction in the computation time compared to
 existing methods and the use of trivial unfitted Cartesian meshes that
 are independent of irregular geometry, the proposed technique does
 not require remeshing for the shape change of irregular geometry
 and it will be effective for many design and optimization problems as
 well as for multiscale problems without the scale separation.

In the future we plan to develop OLTEM with adaptive mesh refinement similar to h- and p- mesh refinements for finite elements (e. g., it was shown in papers [31,33] that OLTEM can easily combine different stencils). We plan to use quadtrees/octrees meshes that allow a simple refinement strategy with Cartesian meshes. The extension of OLTEM to other PDEs with discontinuous coefficients as well as to non-linear PDEs will be also considered in the future. We plan to extend the new post-processing procedure with OLTEM to other PDEs including accurate stress calculations for elasticity equations.

Declaration of Competing Interest

The authors declare that they have no known competing financial interests or personal relationships that could have appeared to influence the work reported in this paper.

Acknowledgments

The research has been supported in part by the Army Research Office (Grant Number W911NF-21-1-0267), the NSF grant CMMI-1935452 and by Texas Tech University. The views and conclusions contained in this paper are those of the authors and should not be interpreted as representing the official policies.

Appendix A. The coefficients b_p used in Eq. (16) for the 27-point stencils.

The first 10 coefficients b_p (p = 1, 2, ..., 10) are presented below. Please see also Appendix B and the attached file 'b-coef.nb'.

$$\begin{array}{l} b_1 &= \sum_{j=1}^{27} a_j k_j + \sum_{j=1}^{25} q_{1,j} \\ b_2 &= \sum_{j=1}^{27} (1-a_j) k_j - \sum_{j=1}^{25} q_{1,j} \\ b_3 &= \sum_{j=1}^{27} b_z a_j (r_{z,j} - dz_G) k_j + \sum_{j=1}^{25} (d_{z,j} q_{1,j} + e_* n_{z,j} q_{2,j}) \\ b_4 &= \sum_{j=1}^{27} b_z (1-a_j) (r_{z,j} - dz_G) k_j - \sum_{j=1}^{25} (d_{z,j} q_{1,j} + e_{**} n_{z,j} q_{2,j}) \\ b_5 &= \sum_{j=1}^{27} b_y a_j (r_{y,j} - dy_G) k_j + \sum_{j=1}^{25} (d_{y,j} q_{1,j} + e_{**} n_{y,j} q_{2,j}) \\ b_6 &= \sum_{j=1}^{27} b_y (1-a_j) (r_{y,j} - dy_G) k_j - \sum_{j=1}^{25} (d_{y,j} q_{1,j} + e_{**} n_{y,j} q_{2,j}) \\ b_7 &= \sum_{j=1}^{27} b_x a_j (r_{x,j} - dx_G) k_j + \sum_{j=1}^{25} (d_{x,j} q_{1,j} + e_{**} n_{x,j} q_{2,j}) \\ b_8 &= \sum_{j=1}^{27} b_x (1-a_j) (r_{x,j} - dx_G) k_j - \sum_{j=1}^{25} (d_{x,j} q_{1,j} + e_{**} n_{x,j} q_{2,j}) \\ b_9 &= \sum_{j=1}^{27} \frac{1}{2} a_j [b_z^2 (r_{z,j} - dz_G)^2 - (r_{x,j} - dy_G)^2] k_j + \sum_{j=1}^{25} \left[\frac{1}{2} (d_{z,j}^2 - d_{x,j}^2) q_{1,j} + e_* (d_{z,j} n_{x,j} - d_{z,j} n_{x,j}) q_{2,j} \right] \\ b_{10} &= \sum_{j=1}^{27} \frac{1}{2} (1-a_j) [b_z^2 (r_{z,j} - dz_G)^2 - (r_{x,j} - dy_G)^2] k_j - \sum_{j=1}^{25} \left[\frac{1}{2} (d_{z,j}^2 - d_{x,j}^2) q_{1,j} + e_{**} (d_{z,j} n_{x,j} - d_{z,j} n_{x,j}) q_{2,j} \right] \end{array}$$

Appendix B. The explicit form of Eqs. (24) for the determination of the stencil coefficients.

The coefficients b_i in Eq. (16) can be represented as a linear function of the stencil coefficients k_j , $q_{1,j}$ and $q_{1,j}$ as follows:

$$b_i = \sum_{i=1}^{27} s_{ij} k_j + \sum_{i=1}^{25} \left(c_{ij}^1 q_{1,j} + c_{ij}^2 q_{2,j} \right), \qquad i = 1, 2, ..., 98,$$
(B.1)

where the coefficients s_{ij} , c_{ij}^2 and c_{ij}^2 can be found from the expressions for the coefficients b_i ; see Appendix A and the attached file 'b-coef.nb'. Then using Eq. (B.1), the local system of linear algebraic equations for finding the stencil coefficients, Eq. (24), can be rewritten as follows:

$$\frac{\partial \overline{R}}{\partial k_{m}} = \sum_{l=1}^{32} \lambda_{l} \frac{\partial b_{l}}{\partial k_{m}} + 2 \left[\sum_{p=33}^{50} b_{p} \frac{\partial b_{p}}{\partial k_{m}} + h_{1} \sum_{p=51}^{72} b_{p} \frac{\partial b_{p}}{\partial k_{m}} + h_{2} \sum_{p=73}^{98} b_{p} \frac{\partial b_{p}}{\partial k_{m}} \right]$$

$$= \sum_{l=1}^{32} \lambda_{l} s_{lm} + 2 \left[\sum_{j=1}^{27} \left(\sum_{p=33}^{50} s_{pj} s_{pm} + h_{1} \sum_{p=51}^{72} s_{pj} s_{pm} + h_{2} \sum_{p=73}^{98} s_{pj} s_{pm} \right) k_{j} \right]$$

$$+ \sum_{j=1}^{25} \left(\sum_{p=33}^{50} c_{pj}^{1} s_{pm} + h_{1} \sum_{p=51}^{72} c_{pj}^{1} s_{pm} + h_{2} \sum_{p=73}^{98} c_{pj}^{1} s_{pm} \right) q_{1,j} + \sum_{j=1}^{25} \left(\sum_{p=33}^{50} c_{pj}^{2} s_{pm} + h_{1} \sum_{p=51}^{72} c_{pj}^{2} s_{pm} + h_{2} \sum_{p=73}^{98} c_{pj}^{2} s_{pm} \right) q_{2,j} \right] = 0,$$

$$m = 1, 2, ..., 27,$$

$$\frac{\partial \overline{R}}{\partial q_{1,m}} = \sum_{l=1}^{32} \lambda_l \frac{\partial b_l}{\partial q_{1,m}} + 2 \left[\sum_{p=33}^{50} b_p \frac{\partial b_p}{\partial q_{1,m}} + h_1 \sum_{p=51}^{72} b_p \frac{\partial b_p}{\partial q_{1,m}} + h_2 \sum_{p=73}^{98} b_p \frac{\partial b_p}{\partial q_{1,m}} \right] \\
= \sum_{l=1}^{32} \lambda_l c_{lm}^1 + 2 \left[\sum_{j=1}^{27} \left(\sum_{p=33}^{50} s_{pj} c_{pm}^1 + h_1 \sum_{p=51}^{72} s_{pj} c_{pm}^1 + h_2 \sum_{p=73}^{98} s_{pj} c_{pm}^1 \right) k_j \right] \\
+ \sum_{j=1}^{25} \left(\sum_{p=33}^{50} c_{pj}^1 c_{pm}^1 + h_1 \sum_{p=51}^{72} c_{pj}^1 c_{pm}^1 + h_2 \sum_{p=73}^{98} c_{pj}^1 c_{pm}^1 \right) q_{1,j} + \sum_{j=1}^{25} \left(\sum_{p=33}^{50} c_{pj}^2 c_{pm}^1 + h_1 \sum_{p=51}^{72} c_{pj}^2 c_{pm}^1 + h_2 \sum_{p=73}^{98} c_{pj}^2 c_{pm}^1 \right) q_{2,j} = 0, \\
m = 1, 2, \dots, 25.$$

$$\frac{\partial \overline{R}}{\partial q_{2,m}} = \sum_{l=1}^{32} \lambda_l \frac{\partial b_l}{\partial q_{2,m}} + 2 \left[\sum_{p=33}^{50} b_p \frac{\partial b_p}{\partial q_{2,m}} + h_1 \sum_{p=51}^{72} b_p \frac{\partial b_p}{\partial q_{2,m}} + h_2 \sum_{p=73}^{98} b_p \frac{\partial b_p}{\partial q_{2,m}} \right] \\
= \sum_{l=1}^{32} \lambda_l c_{lm}^2 + 2 \left[\sum_{j=1}^{27} \left(\sum_{p=33}^{50} s_{pj} c_{pm}^2 + h_1 \sum_{p=51}^{72} s_{pj} c_{pm}^2 + h_2 \sum_{p=73}^{98} s_{pj} c_{pm}^2 \right) k_j \right] \\
+ \sum_{j=1}^{25} \left(\sum_{p=33}^{50} c_{pj}^1 c_{pm}^2 + h_1 \sum_{p=51}^{72} c_{pj}^1 c_{pm}^2 + h_2 \sum_{p=73}^{98} c_{pj}^2 c_{pm}^2 \right) q_{1,j} + \sum_{j=1}^{25} \left(\sum_{p=33}^{50} c_{pj}^2 c_{pm}^2 + h_1 \sum_{p=51}^{72} c_{pj}^2 c_{pm}^2 + h_2 \sum_{p=73}^{98} c_{pj}^2 c_{pm}^2 \right) q_{2,j} = 0, \\
m = 1, 2, \dots, 25,$$

$$\frac{\partial \overline{R}}{\partial \lambda_m} = b_m = \sum_{i=1}^{27} s_{mj} k_j + \sum_{i=1}^{25} \left(c_{mj}^1 q_{1,j} + c_{mj}^2 q_{2,j} \right) = 0, \qquad m = 1, 2, \dots, 32,$$
(B.5)

where Eqs. (B.2)–(B.5) form a system of 109 linear algebraic equations for the determination of the stencil coefficients k_j (j = 1, 2, ..., 27), $q_{1,j}$ and $q_{2,j}$ (j = 1, 2, ..., 25) as well as 32 Lagrange multiplier λ_l (l = 1, 2, ..., 32).

Appendix C. The coefficients k_i (i = 1, 2, ..., 27) of the 27-point uniform stencils for homogeneous materials

$$k_{1} = \frac{(5(b_{c}^{2}+1)b_{y}^{2}+5b_{c}^{2}+9)}{8(125(b_{c}^{2}+1)b_{y}^{2}+125b_{c}^{2}+9)}, \qquad k_{2} = \frac{(5(b_{c}^{2}-5)b_{y}^{2}-25b_{c}^{2}+9)}{500(b_{c}^{2}+1)b_{y}^{2}+500b_{c}^{2}+36},$$

$$k_{3} = -\frac{(5(b_{c}^{2}+1)b_{y}^{2}+5b_{c}^{2}+9)}{8(125(b_{c}^{2}+1)b_{y}^{2}+125b_{c}^{2}+9)}, \qquad k_{4} = \frac{(-25(b_{c}^{2}+1)b_{y}^{2}+5b_{c}^{2}+9)}{500(b_{c}^{2}+1)b_{y}^{2}+500b_{c}^{2}+36},$$

$$k_{5} = \frac{(25(b_{c}^{2}-5)b_{y}^{2}+25b_{c}^{2}-9)}{250(b_{c}^{2}+1)b_{y}^{2}+250b_{c}^{2}+18}, \qquad k_{6} = \frac{(-25(b_{c}^{2}+1)b_{y}^{2}+5b_{c}^{2}+9)}{500(b_{c}^{2}+1)b_{y}^{2}+500b_{c}^{2}+36},$$

$$k_{7} = \frac{(5(b_{c}^{2}+1)b_{y}^{2}+5b_{c}^{2}+9)}{8(125(b_{c}^{2}+1)b_{y}^{2}+5b_{c}^{2}+9)}, \qquad k_{8} = \frac{(5(b_{c}^{2}-5)b_{y}^{2}-25b_{c}^{2}+9)}{500(b_{c}^{2}+1)b_{y}^{2}+500b_{c}^{2}+36},$$

$$k_{9} = -\frac{(5(b_{c}^{2}+1)b_{y}^{2}+5b_{c}^{2}+9)}{8(125(b_{c}^{2}+1)b_{y}^{2}+125b_{c}^{2}+9)}, \qquad k_{10} = -\frac{(5(b_{c}^{2}-5)b_{y}^{2}-25b_{c}^{2}-9)}{500(b_{c}^{2}+1)b_{y}^{2}+500b_{c}^{2}+36},$$

$$k_{11} = \frac{(25(b_{c}^{2}+1)b_{y}^{2}+5b_{c}^{2}+9)}{250(b_{c}^{2}+1)b_{y}^{2}+250b_{c}^{2}+18}, \qquad k_{12} = -\frac{(5(b_{c}^{2}-1)b_{y}^{2}+25b_{c}^{2}-9)}{500(b_{c}^{2}+1)b_{y}^{2}+500b_{c}^{2}+36},$$

$$k_{13} = \frac{(-25(b_{c}^{2}-1)b_{y}^{2}+25b_{c}^{2}-9)}{250(b_{c}^{2}+1)b_{y}^{2}+5500b_{c}^{2}+36}, \qquad k_{14} = 1,$$

$$k_{13} = \frac{(5(b_{c}^{2}-1)b_{y}^{2}+25b_{c}^{2}-9)}{500(b_{c}^{2}+1)b_{y}^{2}+500b_{c}^{2}+36},$$

$$k_{13} = \frac{(5(b_{c}^{2}-1)b_{y}^{2}+25b_{c}^{2}-9)}{500(b_{c}^{2}+1)b_{y}^{2}+5500b_{c}^{2}+36},$$

$$k_{13} = \frac{(5(b_{c}^{2}-1)b_{y}^{2}+25b_{c}^{2}-9)}{500(b_{c}^{2}+1)b_{y}^{2}+5500b_{c}^{2}+36},$$

$$k_{13} = \frac{(5(b_{c}^{2}-1)b_{y}^{2}+25b_{c}^{2}-9)}{500(b_{c}^{2}+1)b_{y}^{2}+5500b_{c}^{2}+36},$$

$$k_{14} = \frac{(5(b_{c}^{2}-1)b_{y}^{2}+25b_{c}^{2}-9)}{500(b_{c}^{2}+1)b_{y}^{2}+5500b_{c}^{2}+36},$$

$$k_{14} = \frac{(5(b_{c}^{2}-1)b_{y}^{2}+25b_{c}^{2}-9)}{500(b_{c}^{2}+1)b_{y}^{2}+250b_{c}^{2}+18},$$

$$k_{15} = \frac{(5(b_{c}^{2}-1)b_{y}^{2}+25b_{c}^{2}-9)}{250(b_{c}^{2}+1)b_{y}^{2}+25b_{c}^{2}-9)},$$

$$k_{16} = \frac{(5(b_{c}^{2}-1)b_{y}^{2}+5b_{c}^{2}+9)}{500(b_{c}^{2}$$

Appendix D. The coefficients k_j (j=1,2,...,27) of the 27-point uniform stencils for homogeneous materials used for the calculation of the derivatives $\frac{\partial u^{num}}{\partial x}$, $\frac{\partial u^{num}}{\partial x}$ and $\frac{\partial u^{num}}{\partial z}$

$$k_i$$
 $(j = 1, 2, ..., 27)$ for the calculation of $\frac{\partial u^{num}}{\partial x}$:

$$k_{1} = \frac{7}{360b_{y}^{2}b_{z}^{2}}, \quad k_{2} = 0, \quad k_{3} = -\frac{7}{360b_{y}^{2}b_{z}^{2}}, \quad k_{4} = \frac{15b_{y}^{2} - 7}{180b_{y}^{2}b_{z}^{2}}, \quad k_{5} = 0, \quad k_{6} = \frac{7 - 15b_{y}^{2}}{180b_{y}^{2}b_{z}^{2}},$$

$$k_{7} = \frac{7}{360b_{y}^{2}b_{z}^{2}}, \quad k_{8} = 0, \quad k_{9} = -\frac{7}{360b_{y}^{2}b_{z}^{2}}, \quad k_{10} = \frac{15b_{z}^{2} - 7}{180b_{y}^{2}b_{z}^{2}}, \quad k_{11} = 0, \quad k_{12} = \frac{7 - 15b_{z}^{2}}{180b_{y}^{2}b_{z}^{2}},$$

$$k_{13} = \frac{1}{90} \left(\frac{\frac{7}{b_{z}^{2}} - 15}{b_{y}^{2}} - \frac{15}{b_{z}^{2}} + 45 \right), \quad k_{14} = 0, \quad k_{15} = \frac{1}{90} \left(\frac{15 - \frac{7}{b_{z}^{2}}}{b_{y}^{2}} + 15 \left(\frac{1}{b_{z}^{2}} - 3 \right) \right),$$

$$k_{16} = \frac{15b_{z}^{2} - 7}{180b_{y}^{2}b_{z}^{2}}, \quad k_{17} = 0, \quad k_{18} = \frac{7 - 15b_{z}^{2}}{180b_{y}^{2}b_{z}^{2}}, \quad k_{19} = \frac{7}{360b_{y}^{2}b_{z}^{2}}, \quad k_{20} = 0, \quad k_{21} = -\frac{7}{360b_{y}^{2}b_{z}^{2}},$$

$$k_{22} = \frac{15b_{y}^{2} - 7}{180b_{y}^{2}b_{z}^{2}}, \quad k_{23} = 0, \quad k_{24} = \frac{7 - 15b_{y}^{2}}{180b_{y}^{2}b_{z}^{2}}, \quad k_{25} = \frac{7}{360b_{y}^{2}b_{z}^{2}}, \quad k_{26} = 0, \quad k_{27} = -\frac{7}{360b_{y}^{2}b_{z}^{2}}.$$

 k_i (j = 1, 2, ..., 27) for the calculation of $\frac{\partial u^{num}}{\partial v}$:

$$k_{1} = \frac{b_{y}}{72b_{z}^{2}}, \quad k_{2} = \frac{b_{y}}{18b_{z}^{2}}, \quad k_{3} = \frac{b_{y}}{72b_{z}^{2}}, \quad k_{4} = 0, \quad k_{5} = 0, \quad k_{6} = 0, \quad k_{7} = -\frac{b_{y}}{72b_{z}^{2}},$$

$$k_{8} = -\frac{b_{y}}{18b_{z}^{2}}, \quad k_{9} = -\frac{b_{y}}{72b_{z}^{2}}, \quad k_{10} = \frac{b_{y}(3b_{z}^{2}-1)}{36b_{z}^{2}}, \quad k_{11} = b_{y}\left(-\frac{1}{9b_{z}^{2}} - \frac{1}{6}\right) + \frac{1}{2b_{y}}, \quad k_{12} = \frac{b_{y}(3b_{z}^{2}-1)}{36b_{z}^{2}},$$

$$k_{13} = 0, \quad k_{14} = 0, \quad k_{15} = 0, \quad k_{16} = \frac{b_{y}-3b_{y}b_{z}^{2}}{36b_{z}^{2}}, \quad k_{17} = b_{y}\left(\frac{1}{9b_{z}^{2}} + \frac{1}{6}\right) - \frac{1}{2b_{y}}, \quad k_{18} = \frac{b_{y}-3b_{y}b_{z}^{2}}{36b_{z}^{2}},$$

$$k_{19} = \frac{b_{y}}{72b_{z}^{2}}, \quad k_{20} = \frac{b_{y}}{18b_{z}^{2}}, \quad k_{21} = \frac{b_{y}}{72b_{z}^{2}}, \quad k_{22} = 0, \quad k_{23} = 0, \quad k_{24} = 0, \quad k_{25} = -\frac{b_{y}}{72b_{z}^{2}},$$

$$k_{26} = -\frac{b_{y}}{78b_{z}^{2}}, \quad k_{27} = -\frac{b_{y}}{72b_{z}^{2}}.$$

 k_i (j=1,2,...,27) for the calculation of $\frac{\partial u^{num}}{\partial x}$:

$$k_{1} = \frac{b_{z}}{72b_{y}^{2}}, \qquad k_{2} = \frac{b_{z}}{18b_{y}^{2}}, \qquad k_{3} = \frac{b_{z}}{72b_{y}^{2}}, \qquad k_{4} = \frac{\left(3b_{y}^{2} - 1\right)b_{z}}{36b_{y}^{2}}, \qquad k_{5} = \left(-\frac{1}{9b_{y}^{2}} - \frac{1}{6}\right)b_{z} + \frac{1}{2b_{z}},$$

$$k_{6} = \frac{\left(3b_{y}^{2} - 1\right)b_{z}}{36b_{y}^{2}}, \qquad k_{7} = \frac{b_{z}}{72b_{y}^{2}}, \qquad k_{8} = \frac{b_{z}}{18b_{y}^{2}}, \qquad k_{9} = \frac{b_{z}}{72b_{y}^{2}}, \qquad k_{10} = 0, \qquad k_{11} = 0, \qquad k_{12} = 0,$$

$$k_{13} = 0, \qquad k_{14} = 0, \qquad k_{15} = 0, \qquad k_{16} = 0, \qquad k_{17} = 0, \qquad k_{18} = 0, \qquad k_{19} = -\frac{b_{z}}{72b_{y}^{2}}, \qquad k_{20} = -\frac{b_{z}}{18b_{y}^{2}},$$

$$k_{21} = -\frac{b_{z}}{72b_{y}^{2}}, \qquad k_{22} = \frac{b_{z} - 3b_{y}^{2}b_{z}}{36b_{y}^{2}}, \qquad k_{23} = \left(\frac{1}{9b_{y}^{2}} + \frac{1}{6}\right)b_{z} - \frac{1}{2b_{z}}, \qquad k_{24} = \frac{b_{z} - 3b_{y}^{2}b_{z}}{36b_{y}^{2}}, \qquad k_{25} = -\frac{b_{z}}{72b_{y}^{2}},$$

$$k_{26} = -\frac{b_{z}}{18b_{y}^{2}}, \qquad k_{27} = -\frac{b_{z}}{72b_{y}^{2}}.$$

Supplementary material

Supplementary material associated with this article can be found, in the online version, at doi: 10.1016/j.advengsoft.2022.103103.

References

- [1] Vallaghe S, Papadopoulo T. A trilinear immersed finite element method for solving the electroencephalography forward problem. SIAM J Sci Comput 2010;32(4): 2379–94.
- [2] Crockett R, Colella P, Graves D. A Cartesian grid embedded boundary method for solving the poisson and heat equations with discontinuous coefficients in three dimensions. J Comput Phys 2011;230(7):2451–69.
- [3] Zhang Q, Ito K, Li Z, Zhang Z. Immersed finite elements for optimal control problems of elliptic PDEs with interfaces. J Comput Phys 2015;298:305–19.
- [4] Guittet A, Lepilliez M, Tanguy S, Gibou F. Solving elliptic problems with discontinuities on irregular domains - the Voronoi interface method. J Comput Phys 2015;298:747–65.
- [5] Coco A, Russo G. Second order finite-difference ghost-point multigrid methods for elliptic problems with discontinuous coefficients on an arbitrary interface. J Comput Phys 2018;361:299–330.
- [6] Gürkan C, Massing A. A stabilized cut discontinuous Galerkin framework for elliptic boundary value and interface problems. Comput Methods Appl Mech Eng 2019;348:466–99
- [7] Zhang Q, Babuska I. A stable generalized finite element method (SGFEM) of degree two for interface problems. Comput Methods Appl Mech Eng 2020;363:112889.
- [8] Guo R, Lin T. An immersed finite element method for elliptic interface problems in three dimensions. J Comput Phys 2020:414:109478.
- [9] Li K, Atallah NM, Main GA, Scovazzi G. The shifted interface method: a flexible approach to embedded interface computations. Int J Numer Methods Eng 2020;121 (3):492–518.
- [10] Xiao Y, Xu J, Wang F. High-order extended finite element methods for solving interface problems. Comput Methods Appl Mech Eng 2020;364:112964.
- [11] Vos P, van Loon R, Sherwin S. A comparison of fictitious domain methods appropriate for spectral/hp element discretisations. Comput Methods Appl Mech Eng 2008;197(25–28):2275–89.
- [12] Burman E, Hansbo P. Fictitious domain finite element methods using cut elements: I. A stabilized lagrange multiplier method. Comput Methods Appl Mech Eng 2010; 199(41–44):2680–6.
- [13] Rank E, Kollmannsberger S, Sorger C, Duster A. Shell finite cell method: a high order fictitious domain approach for thin-walled structures. Comput Methods Appl Mech Eng 2011;200(45–46):3200–9.
- [14] Rank E, Ruess M, Kollmannsberger S, Schillinger D, Duster A. Geometric modeling, isogeometric analysis and the finite cell method. Comput Methods Appl Mech Eng 2012;249–252:104–15.

- [15] May S, Berger M. An explicit implicit scheme for cut cells in embedded boundary meshes. J Sci Comput 2017;71(3):919–43.
- [16] Main A, Scovazzi G. The shifted boundary method for embedded domain computations. Part I: Poisson and stokes problems. J Comput Phys 2017.
- [17] Song T, Main A, Scovazzi G, Ricchiuto M. The shifted boundary method for hyperbolic systems: embedded domain computations of linear waves and shallow water flows. J Comput Phys 2018;369:45–79.
- [18] Kreisst H-O, Petersson NA. An embedded boundary method for the wave equation with discontinuous coefficients. SIAM J Sci Comput 2006;28(6):2054–74.
- [19] Kreiss H-O, Petersson NA. A second order accurate embedded boundary method for the wave equation with Dirichlet data. SIAM J Sci Comput 2006;27(4):1141–67.
- [20] Kreiss H-O, Petersson NA, Ystrom J. Difference approximations of the Neumann problem for the second order wave equation. SIAM J Numer Anal 2004;42(3): 1292–233
- [21] McCorquodale P, Colella P, Johansen H. A Cartesian grid embedded boundary method for the heat equation on irregular domains. J Comput Phys 2001;173(2): 620–35
- [22] Johansen H, Colella P. A Cartesian grid embedded boundary method for Poisson's equation on irregular domains. J Comput Phys 1998;147(1):60–85.
- [23] Guo R, Lin T. A higher degree immersed finite element method based on a cauchy extension for elliptic interface problems. SIAM J Numer Anal 2019;57(4):1545–73.
- [24] Cheung J, Gunzburger M, Bochev P, Perego M. An optimally convergent higherorder finite element coupling method for interface and domain decomposition problems. Results Appl Math 2020;6:100094.
- [25] Neiva E, Badia S. Robust and scalable h-adaptive aggregated unfitted finite elements for interface elliptic problems. Comput Methods Appl Mech Eng 2021; 380:113769.
- [26] Badia S, Neiva E, Verdugo F. Linking ghost penalty and aggregated unfitted methods. Comput Methods Appl Mech Eng 2022;388:114232.
- [27] Idesman A. A new numerical approach to the solution of PDEs with optimal accuracy on irregular domains and Cartesian meshes. Part 1: the derivations for the wave, heat and poisson equations in the 1-d and 2-d cases. Arch Appl Mech 2020; 90(12):2621–48.
- [28] Dey B, Idesman A. A new numerical approach to the solution of PDEs with optimal accuracy on irregular domains and Cartesian meshes. Part 2: numerical simulation and comparison with FEM. Arch Appl Mech 2020;90(12):2649–74.
- [29] Idesman A, Dey B. A new 3-D numerical approach to the solution of PDEs with optimal accuracy on irregular domains and Cartesian meshes. Comput Methods Appl Mech Eng 2019;354:568–92.

- [30] Idesman A, Dey B. Compact high-order stencils with optimal accuracy for numerical solutions of 2-D time-independent elasticity equations. Comput Methods Appl Mech Eng 2020;360:1–17.
- [31] Idesman A, Dey B. Accurate numerical solutions of 2-D elastodynamics problems using compact high-order stencils. Comput Struct 2020;229:1–18.
- [32] Idesman A, Dey B. A new numerical approach to the solution of the 2-D Helmholtz equation with optimal accuracy on irregular domains and Cartesian meshes. Comput Mech 2020;65:1189–204.
- [33] Idesman A, Dey B. New 25-point stencils with optimal accuracy for 2-D heat transfer problems. Comparison with the quadratic isogeometric elements. J Comput Phys 2020;418:109640.
- [34] Idesman A, Dey B. Optimal local truncation error method for solution of wave and heat equations for heterogeneous materials with irregular interfaces and unfitted Cartesian meshes. Comput Methods Appl Mech Eng 2021;384:113998.
- [35] Idesman A, Dey B. 3-rd and 11th orders of accuracy of 'linear' and 'quadratic' elements for the Poisson equation with irregular interfaces on unfitted Cartesian meshes. Int J Numer Methods Heat Fluid Flow 2021:1–31.

- [36] Zienkiewicz OC, Zhu JZ. The superconvergent patch recovery and a posteriori error estimates. Part 1: the recovery technique. Int J Numer Methods Eng 1992;33(7): 1331–64.
- [37] Zienkiewicz OC, Zhu JZ. The superconvergent patch recovery and a posteriori error estimates. Part 2: error estimates and adaptivity. Int J Numer Methods Eng 1992;33 (7):1365–82.
- [38] Kumar M, Kvamsdal T, Johannessen KA. Superconvergent patch recovery and a posteriori error estimation technique in adaptive isogeometric analysis. Comput Methods Appl Mech Eng 2017;316:1086–156. Special Issue on Isogeometric Analysis: Progress and Challenges
- [39] Idesman A, Dey B. The treatment of the Neumann boundary conditions for a new numerical approach to the solution of PDEs with optimal accuracy on irregular domains and Cartesian meshes. Comput Methods Appl Mech Eng 2020;365: 112985.
- [40] Bathe KJ. Finite element procedures. Upper Saddle River, New Jersey: Prentice-Hall Inc.; 1996.
- [41] Langtangen HP, Linge S. Finite difference computing with PDEs. Springer; 2017.